MINERAL TRANSFORMATION, ALKALINITY NEUTRALIZATION AND SETTLING OF A LONG-TERM STORAGE BAUXITE RESIDUE

A Thesis

by

CHIAWEI LIN

Submitted to the Office of Graduate and Professional Studies of
Texas A&M University
in partial fulfillment of the requirements for the degree of

MASTER OF SCIENCE

Chair of Committee,	Youjun Deng
Committee Members,	Julie Howe
	Kevin McInnes
	Marcelo Sanchez-Castilla
Head of Department,	David D. Baltensperger

May 2021

Major Subject: Soil Science

Copyright 2021 Chiawei Lin

ABSTRACT

Over 4 billion tonnes of bauxite residue, the by-product of alumina refinery, has been generated globally. High alkalinity and high-water content of the residues are two of the major challenges in dealing with its safe storage and management. Limited studies have evaluated the treatments of neutralization of the alkalinity of long-term storage bauxite residues and the enhanced settling performance after alkalinity neutralization simultaneously. The objectives of this study were to: 1) investigate the mineral compositions and transformation of a wet bauxite residue in a more-than-50-year old storage pond, 2) examine the efficiencies of four compounds: H_2SO_4, $CaCl_2$, $FeCl_3$, and NaH_2PO_4 in neutralizing alkalinity; and 3) evaluate the effectiveness of the above treatments with and without additional surfactants and polymers in enhancing the settling of bauxite residues.

Mineral quantification indicated that Fe-oxides dominated the land area residue and lower portion of the lake sediments whereas aluminum hydroxides/oxyhydroxide dominated the upper portion of the sediment. The uncommon dominance of Al-hydroxide could be attributed to precipitation of the bayerite and nordstrandite [$Al(OH)_3$] at lower pH when atmospheric CO_2 dissolved in lake water reducing the pH of the residue during storage. The precipitation of aluminum hydroxide created an Al concentration gradient, drove aluminate ions from lower sediments to diffuse upward in the bauxite deposit column. This also explained the formation of a hard surface crust, consisting of bayerite, nordstrandite, and calcite, at the disposal pond land area.

The four chemicals (i.e., H_2SO_4, $CaCl_2$, $FeCl_3$, and NaH_2PO_4) successfully reduced the pH of the bauxite residue from 10 to 8, but none of them improved the settling of the residue compared to the NaCl control treatment. Anionic surfactant (SDS) improved the settling of bauxite residue before but not after alkalinity neutralization. Neutral and anionic polyacrylamide (PAM) promoted the flocculation and settling of bauxite residue both before and after alkalinity neutralization, while cationic PAM showed little effect. It appeared that binding phosphate on the surfaces of oxides altered the surface properties of bauxite residue and reduced the PAM settling efficiency.

Among the surfactant and polymers tested, anionic and nonionic polyacrylamide enhanced the settling of residue by forming larger flocs more quickly. Forming stable large flocs also promoted the formation of large pores, which hindered the consolidation of the particles to smaller volumes.

ACKNOWLEDGEMENTS

I would like to thank my committee chair, Dr. Deng, and my committee members, Dr. Howe, Dr. McInnes and Dr. Sanchez, for their guidance and support throughout the course of this research.

Thanks also go to my friends and colleagues and the department faculty and staff for making my time at Texas A&M University a great experience.

Finally, thanks to my mother and father for their encouragement, patience and love.

CONTRIBUTORS AND FUNDING SOURCES

Contributors

This work was supervised by a thesis committee consisting of Professors Youjun Deng, Kevin McInnes and Julie Howe of the Department of Soil and Crop Sciences and Professor Marcelo Sanchez-Castilla of the Department of Civil and Environmental Engineering.

The lake water was analyzed by Soil, Water and Forage Testing Lab, Texas A&M AgriLife Extension Service. All other work conducted for the thesis was completed by the student independently.

Funding Sources

Graduate study was partially supported by the Excellence Fellowship in the College of Agriculture and Life Sciences at Texas A&M University.

This work was also made possible in part by a private company. Its contents are solely the responsibility of the authors and do not necessarily represent the official views of the company.

NOMENCLATURE

Al	Aluminum
ATR	Attenuated Total Reflection
BDTDA	Benzyldimethyltetradecylammonium chloride
BR	Bauxite residue
BPCSs	Bayer process characteristic solids
$CaCl_2$	Calcium chloride
DI water	Distilled water
DLVO theory	Derjaguin, Landau, Verwey, and Overbeek theory
EC	Electrical conductivity (mS cm^{-1})
Fe	Iron
FTIR	Fourier-transform infrared spectroscopy
H_2SO_4	Sulfuric acid
ICSD	Inorganic Crystal Structure Database
kV	Kilovolt
mA	Milliamp
$MgCl_2$	Magnesium chloride
NaCl	Sodium chloride
NaH_2PO_4	Monosodium phosphate
NaOH	Sodium hydroxide
NIST	National Institute of Standards and Technology
PAM	Polyacrylamide

PZC	Point of zero charge
Rwp	Weighted pattern R-value
SDS	Sodium dodecyl sulfate
SEM	Scanning electron microscope
XRD	X-ray diffraction

TABLE OF CONTENTS

Page

LIST OF FIGURES

Page

LIST OF TABLES

Page

1. INTRODUCTION

1.1. Background

Refining bauxite ore to aluminum hydroxides (gibbsite or bayerite) for metallic aluminum production through the Bayer process generates roughly 120 million tonnes of residue per annum globally[1]. In the Bayer process, aluminum hydroxides [$Al(OH)_3$] and oxyhydroxides (AlOOH) are dissolved by a sodium hydroxide solution under elevated temperatures and pressures. After separating the soluble aluminum species, the insoluble phases and trapped solution become bauxite residue wastes. The residues contain iron oxides: hematite (Fe_2O_3) and goethite (FeOOH); titanium oxides: anatase (TiO_2), rutile (TiO_2), ilmenite ($FeTiO_3$), and perovskite ($CaTiO_3$); undissolved boehmite (AlOOH), gibbsite [$Al(OH)_3$], and quartz (SiO_2); and entrapped alkaline liquor. The residues are typically stored in disposal impoundments[2, 3]. Improper management of the residues often leads disasters to the environment and society[4]. For example, the Ajka alumina plant accident contaminated approximately 120 km downstream rivers and about 800 ha of agricultural land in Hungary in 2010[5, 6]. Treating and utilizing the bauxite residues have been a long-term goal of the aluminum industry since the beginning of the Bayer process started more than a century ago.

Various attempts have been made to utilize bauxite residues, such as converting them to building construction materials, catalysts, coatings, and pigments[1, 7]. In practice, however, all uses of the residues account for less than 3 %[2] of the over 4 billion bauxite residue inventories that have been accumulated around the world[8]. The majority of the

residues remains in storage ponds or layers needing management or treatment. It is critical to develop more efficient methods to increase the storage capacity of the pond/lagoon facilities and to secure the residues by increasing their stability.

The high-water holding capacity, high alkalinity, fine particle size, and considerable specific surface areas of the iron oxides and aluminum (oxy)hydroxides of the bauxite residue are the major limiting factors in their settling, dewatering, and forming stable aggregates[2, 9, 10]. This is especially true for the old storage facilities when wet bauxite residue was pumped to the storage ponds directly. Efficient and economical ways to neutralize the alkalinity and to improve the settling of the minerals in the residue are crucial before the wet residues' dewatering and stabilization. The general goals of this study are to 1) understand the residue mineral changes during the storage, 2) develop strategies to neutralize their alkalinity, and 3) improve the settling of bauxite residues in the storage facility.

Many approaches have been proposed to reduce the water content and to neutralize the alkalinity of bauxite residues, but only a few are used in practice. To increase the solid content prior deposition, bauxite residues are thickened by vacuum or high-pressure filtration[7]. Seawater[11], strong acids[12], gypsum,[13] and carbon dioxide[14] have been proposed to be used to neutralize the alkalinity of bauxite residues.

It is also noteworthy that there were many reports on the alkalinity neutralization of the "fresh" bauxite residues, but only limited studies evaluated the potentials of treatments for alkalinity neutralization on the settling performance of long-term storage bauxite residues. The objectives of this study are to 1) investigate the mineral

compositions and transformation of a wet bauxite residue in a more-than-50-year old undisclosed storage pond; 2) examine the efficiencies of four compounds: sulfuric acid, calcium chloride, iron chloride, and sodium phosphate in neutralizing the alkalinity of the residue; and 3) evaluate the effectiveness of the above treatments with and without additional surfactants and polymers in the settling of bauxite residues during alkalinity neutralization.

Our hypotheses were that 1) the Ca^{2+} and Mg^{2+} ions may form carbonate minerals with the bicarbonate and carbonate anions in the residue slurries to neutralize the alkalinity; 2) the polyvalent cations (Ca^{2+}, Fe^{3+}) may reduce the double layer thickness of oxides, and phosphate may cement the iron oxides and aluminum oxides in the residue. These two processes could improve the aggregation and settling of the residue; and 3) surfactants and polymers could change surface hydrophobicity and inter-particle networking, thus modifying the flocculation and settling of the particles.

1.2. Common disposal and storage techniques

Dewatering of high-water content mine tailings is a ubiquitous problem in many industries, such as coal, phosphate, copper, oil sands, and alumina production[15]. In general, external (thermal, mechanical, electric, or other form) energy is required to reduce the water content of the tailing. Dewatering by natural desiccation, centrifugation, filtration, and electro-filtration have been examined[15]. Exclusion of water out of the tailings is another option. Freeze-thaw, gelation, and water absorbents are

three examples of this option. These methods, however, are still under development in the lab and they work only in confined environments.

Only a few dewatering technologies are practical on an industrial scale. Natural drying such as thin-lift drying and deep in-pit deposition are relatively economical, but it requires large land areas and is limited by weather conditions. Centrifugation and filtration are commonly used in mineral processing, but they are rarely used in bauxite residue dewatering due to their high operating cost.

1.3. Bauxite residues storage methods evolved

Before 1970s, marine discharge and lagooning were the only two approaches to dispose bauxite residue. The residue slurry was simply transported from washing circuit to the sea via a pipeline and to the lagoon-type impoundment with a low solid content (18-30 wt.%), respectively. After the 70s, the lack of lagoon storage land and the desire to achieve higher recoveries of soda and alumina pushed industries to dewater the bauxite residue before disposal, and the “Dry stacking method” was introduced. Thickening the slurry to paste prior to discharge, dewatering and air-drying by slope in the lagoon can increase the solid content to approximately 50 % by mass. From the 1980s, more plants shifted from the lagooning to the dry stacking method with the latter method increasing in usage from 43% in 1985 to 70% in 2007. To further increase the solid content (> 65 wt.%), successful filtration by drum filter, plate and frame filters have been employed in some plants. The application is still limited. Currently, interest in

bauxite residue management is shifting toward remediation and rehabilitation for closed bauxite residue disposal impoundment[2, 16].

1.4. Alkalinity neutralization and settling of bauxite residue wastes

1.4.1. Alkalinity neutralization of bauxite residue wastes

Double layer theory is a well-known method in describing the surface charge structure in colloid systems[17]. The double layer thickness of a symmetrical electrolyte in the solution is:

$$\frac{1}{\kappa} = \frac{3*10^{-8}}{z*c^{1/2}}\ (cm)$$

where *z* is the valency of ion, and *c* is the electrolyte concentration in molarity[18].

Monovalent cation (i.e., sodium, from sodium hydroxide used in the Bayer process) increases the double layer thickness of bauxite residue particles, which induces dispersion of the particles. High pH of remained Bayer liquor induces more negative charge on Fe and Al oxide residues, causing more dispersion. Thus, the high alkalinity of bauxite residue hampers sedimentation. Adding calcium or magnesium to form hydroxide and carbonate minerals and adding a source of acidity are the two general methods in alkalinity neutralization[19]. Seawater neutralization, based on the first mechanism, reduces the alkalinity by forming calcium and magnesium hydroxide or carbonate minerals[20]. Mineral acids, carbon dioxide, and sulfur dioxide could serve as sources of acid in refinery plants to reduce the alkalinity[16]. Although mineral acids may activate the formation of macro-aggregate in fresh bauxite residue[21], reducing pH (pH =2, 3, 4) did not enhance the settling of the residues[22].

1.4.1.1. Adding polyvalent cations

In waste-water treatment, adding metal inorganic salts with polyvalent cations as the coagulants is one of the widely used approach[23]. At alkaline pH, net negative charge generated from the hydroxyl group on the suspended particle surface and coulombic repulsion forces between colloids stabilize the dispersion. Based on the DLVO theory, particles could contact with each other after overcoming the energy barrier created by the difference between repulsion and attractive forces in the double layer. To destabilize the suspended colloids, charge neutralization is a feasible way to diminish the repulsion force by adsorbing the counterions on the surface[24]. One of efficient hydrolyzing coagulants that can neutralize the negative charge is ferric chloride. The $FeCl_3$ solution itself is acidic: the hydrolysis of Fe^{3+} can release H^+ to neutralize the alkalinity. The interaction of Fe^{3+} and negative charges on the iron oxide surface at high pH may bridge particles in the residue and promote coagulation and settling[25].

1.4.1.2. Adding phosphate

It is reasonable to believe that bauxite residue particle settling can be adjusted by changing their surface properties. Many studies have found that the interaction of phosphate ions with iron oxide, the main component of bauxite residue, affects the surface properties, i.e., PZC, of the oxide after phosphate adsorption. Moreover, if a phosphate anion is adsorbed by two sites on the surface of two particles, the phosphate adsorption may bridge the particles and enhance flocculation and settling.

It is well-known that anions can be strongly adsorbed on the iron oxides[26]. Phosphate adsorption on bauxite residue varies with pH[27]. At pH 4 or 7, phosphate sorption was governed by either chemical adsorption or formation of metal phosphate precipitates. Under alkaline conditions (pH = 10), the chemisorption on Fe-Al phases of bauxite residue was the major phosphate sorption mechanism. No report is available on the effect of phosphate on bauxite residue settling. Due to the high adsorption capacity[28], surfaces of hematite and goethite are expected to be cemented by phosphate, which would further facilitate the settling process.

1.4.2. Improving the settling of alkalinity neutralized bauxite residue

1.4.2.1. Adding polymers

Flocculating colloidal particles by polymers are commonly used in a variety of industries such as aluminum refinery, paper, mining, and water treatment. In the Bayer process, flocculants are added to thicken the bauxite residue during the washing process[10]. Starch was widely used in the early years, but the industries move toward synthetic flocculants, such as polyacrylate and polyacrylamide since 1980s[2]. Many polymer products are available on the market, and the selection of a polymer is determined by aggregation performance, solubility, cost, stability, and others. Some intrinsic properties of polymers are crucial for evaluating the flocculation ability, including molecular weight, charge density, and conformation.

Interactions between polymer and particles can be explained by the interparticle bridging mechanism, which could be further represented by a two-step pathway. The

polymer chains are adsorbed by the particles and bridge the particles initially, then the flocs mature or reconfigure. For the starting adsorption, three possible bonding forces can be exerted between the polymer and the particles: 1) electrostatic interaction, 2) hydrogen bonding, or 3) divalent cation bonding. Electrostatic attraction occurs between cationic polyelectrolytes and negatively charged particles. Hydrogen bonding between the amide and carboxyl group on PAM and the OH or O in structures of metal hydroxides. Divalent cation bonding occurs when the enough divalent cations, such as calcium, exist in the solution. Negatively charged polyelectrolyte sites and negative particles could bind together in the presence of cations. By cation bridging, the loop and tail segments of polymers are important in bridging other particles. Thus, if strong binding between polymer and particle occurs, the available loop and tail segments will decrease, reducing the possibility of interparticle connection.

Polyacrylamide (PAM) is a common water-soluble polymer and has broad industrial uses due to its low cost and high effectiveness in many applications. The NH_2 functional group can interact with the negative surface of aluminum or ferric oxides when the pH is higher than the PZC. In addition to the non-ionic one, a variety of PAM copolymer with different amounts of cationic or anionic units are available commercially. Anionic polyacrylamide is stable under the normal pH range due to the low pKa (<4.9) of carboxyl groups. Anionic sites could also be generated by the polyacrylamide hydrolysis under alkaline condition[29].

1.4.2.2. Adding surfactants

Adsorbing surfactants on mineral surfaces alters surface properties, which can be used to control dewatering of the minerals. The efficiency of surfactant appeared to be dependent on charge, length, and concentration and several other factors. It has been reported that mixing ionic and non-ionic surfactants with iron ore fines resulted in significant reduction of moisture content in the residue[30]. Anionic surfactants, such as sodium dodecyl sulphate (SDS), and nonionic poly ethylene oxide 4000 (PEG) were found to be effective in improving the dewatering of iron ore fines. Cationic surfactants, such as cetyl trimethyl ammonium bromide (CTAB), balanced the charge on the mineral surface, but did not improve dewatering of iron ore fines. The following mechanism for surfactant dewatering has been proposed: the hydrophilic heads adhere to the mineral surface and the extension of hydrophobic tails results in decreased surface tension. Water originally traps between the particles are repelled from the surface and release. Excessive addition of the surfactants deteriorate the dewatering ability due to the formation of micelles from excessive surfactant[30]. Decreasing viscosity of flocculate bauxite residues from ionic surfactants could also support the detrimental effect from excess surfactants. When 1 wt% sodium laurate solution was mixed with excess sodium ion, the flocculated solids was notably dispersed. Interestingly, the dispersion effect from surfactants was not applicable to the sea water neutralized bauxite residues[31]. This might be due to the surfactant precipitation caused by calcium ions in the sea water[32].

2. MATERIALS AND METHODS

2.1. Site description and sample collection

A total of 27 core samples were taken from a bauxite residue storage pond at an undisclosed non-operational alumina plant (Figure 2-1). The disposal pond has an area of about 300,000 m^2. One corner of the pond had received bauxite residue and was above the water level. This will be referred to as the "land" portion of the pond. The pond was divided into two land zones (i.e., zones 1 and 2) and three lake zones (i.e., zones 3-5). The land zones were further subdivided into six sub-zones, which were indicated by 1A, 1B, 1C, 2A, 2B, and 2C. Three cores were taken from each sub-zone and the lake zone until reaching the bottom of the pond. Water samples were collected from the lake. Each bauxite residue core was cut to several 45-cm sections and stored in plastic jars separately. For most cores, only the top and bottom sections were analyzed for the basic physical and chemical properties and mineral identification. After survey on the mineralogical and chemical properties of each sample. All sections of core samples from zone 2A, 3, 4, 5 were selected to examine the vertical mineral distribution in the disposal pond.

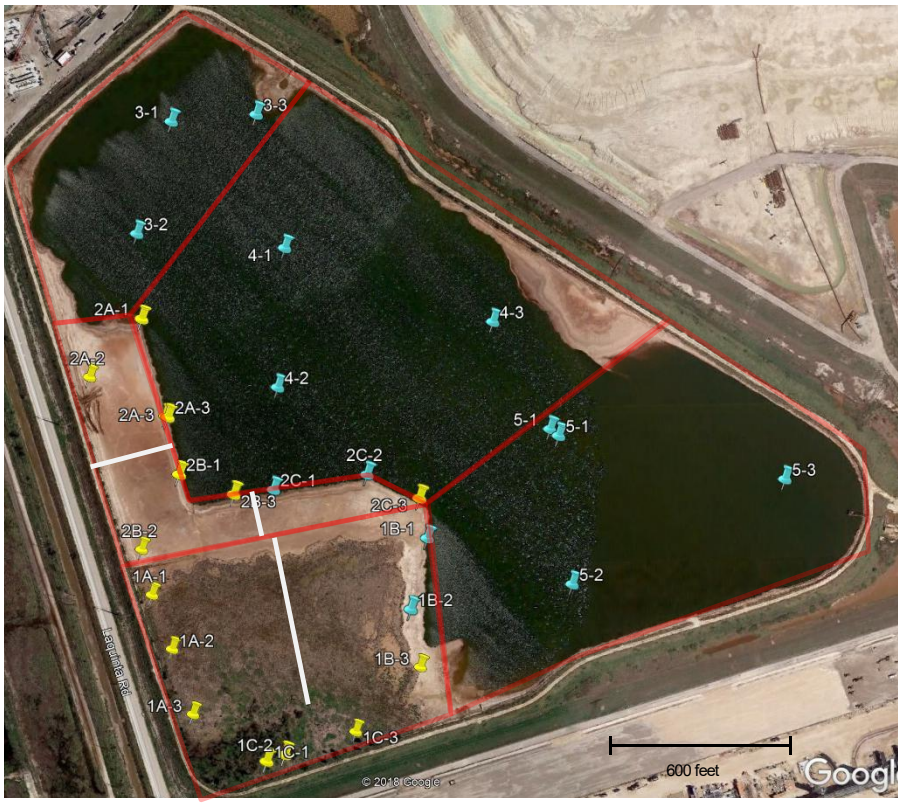

Figure 2-1 Map and sampling sites of bauxite residue disposal pond

2.2. Basic physical and chemical properties

2.2.1. The pH and EC of bauxite residues

For pH and electrical conductivity (EC) measurements, each bauxite residue slurry was mixed with DI water at a 1:2 ratio (wet slurry mass: liquid volume) in a 15-mL centrifuge tube. After 30 minutes of shaking, the samples were centrifuged at 931 xg (m/s^2) for 10 minutes, and pH and EC values of the supernatant were recorded.

2.2.2. Water content of bauxite residues

Gravimetric water content of the residue was determined by oven-drying 10 g wet bauxite residue at 105 °C in a pre-weighed aluminum dish. The water content was then expressed as a percentage of the mass of the oven-dried bauxite residue.

2.2.3. Rapid alkalinity titration and lake water elemental analysis

Twenty grams of wet bauxite residue was mixed with 20 mL DI water or lake water. The mixture was then used in the alkalinity titration with 0.1 M H_2SO_4 solution on a Mettler Toledo T7 titrator, equipped with a Mettler pH-electrode. Visual MINTEQ 3.1 was used to simulate the titration curve. Metal elements in the lake water sample were determined by ICP and the carbonate and bicarbonate contents by acid titration. Water alkalinity was calculated from the carbonate/bicarbonate concentrations. The lake water analysis was conducted by the Soil, Water and Forage Testing Laboratory, Texas A&M AgriLife Extension Service.

2.3. Mineral composition and sample clustering

2.3.1. X-ray diffraction (XRD) analysis

Oven-dried bauxite residue samples were ground to pass through a 0.15-mm sieve. The powders were loaded into a plastic XRD sample holder, and the excess powders were removed with a single sweep by a glass slide. The XRD analysis was conducted on a Bruker D8 with Cu Kα radiation operated at 40 kV and 40 mA. An energy-dispersive detector (Sol-X detector, Bruker) was used to digitally filter out the strong Fe fluorescence from the bauxite residue. X-ray diffraction patterns were

collected from 2° to 70° with a 0.05° 2θ step size and dwell time of 3 seconds at each step.

Mineral identification was verified by matching the XRD peak positions to those of reference minerals in the ICDD PDF-2 database using Bruker EVA program. After mineral phase identification, the Rietveld method was employed with a fundamental parameters approach using Bruker TOPAS software. The LaB6 (SRM 660b) standard from National Institute of Standards and Technology (NIST) was used to constrain instrumental parameters. For real bauxite residue samples, the crystal structure information (initial atomic coordinates, cell parameters, isotropic temperature factors) were obtained from the Inorganic Crystal Structure Database (ICSD). Among all the instrumental parameters, only the specimen displacement parameters needed to be refined. The criteria for the best fit were to minimize the weighted pattern R-value (Rwp).

2.3.2. K-means clustering

After mineral quantification, k-means algorithm was used to partition the samples into k-clusters based on the mineral contents. Briefly, k-means algorithm involves: (1) selecting random initial k centroids; (2) calculating the distance to each centroid for every data point and then assigning the data point to the nearest centroid; and (3) updating the centroid by the average of the data in the same cluster. The above two steps were iterated until convergence[33]. In the original k-means algorithm, choosing the initial centroids were important. Poor initialization may lead to erroneous result. For example, more than one cluster might be assigned to the same centroid. To overcome

this problem, k-means++ was needed to determine the centroids by the distance[34]. In other words, the farthest data point to the current selected centroids will have higher probability to been chosen.

Some limitations exist in k-means algorithm, such as outlier, empty clusters, non-granular shapes and sizes, and number of clusters[33]. Several methods are available to evaluate the optimal number of clusters, including elbow method, silhouette coefficient, gap statistic, and canopy[35]. In the current study, the first two methods were attempted. The principle of elbow method is to calculate the sum of squares from each point to its nearest centroid. When the number of clusters approach optimal number, the sum of squares will converge, which show an "elbow" on the plot. The formula to calculate within-cluster sum of squares is as followed:

$$W_k = \sum_{r=1}^{k} D_r$$

where k is the number of clusters and D_r is the within-cluster sum of squares between all points in a cluster.

Although the elbow method is an efficient way to determine the optimal number of clusters, sometimes the elbow is hard to identify. In this situation, silhouette coefficient method could be used to verify the choice of optimal number of clusters. The concept of silhouette coefficient computes the difference of mean intra cluster distance and mean nearest cluster distance, then divide by the bigger one among these two numbers.

$$S(k) = \frac{b(k) - a(k)}{\max\left[a(k), b(k)\right]}$$

where *a(k)* is the average distance between *k* and all the other data points within the same cluster and *b(k)* is the minimum average distance from *k* to all points in any other cluster.

2.4. ATR-FTIR spectroscopy, scanning electron microscopy and particle size analysis

FTIR spectra of the dried bauxite residues were recorded on a PerkinElmer FTIR system 100 spectrometer using an ATR accessory. All spectra were collected between 650 and 4000 cm^{-1} using 32 scans at a 4-cm^{-1} resolution. Background and blank were recorded in the absence of any substances on the beam path. Post treatments, such as peak labeling or blank signal removal, were performed by software Spectrum from PerkinElmer. Scanning electron microscope images of bauxite residues were acquired with a Quanta 600 FE-SEM (FEI Company) in the Microscopy & Imaging Center at Texas A&M University. Particle size distribution was determined on a Beckman Coulter LS230 laser particle size analyzer (Beckman Coulter, Inc., Fullerton, California).

2.5. Alkalinity neutralization and settling performance

2.5.1. Carbonate formation in bauxite residue liquid simulant when alkalinity was neutralized with Ca^{2+} and Mg^{2+}

To obtain the optimal alkalinity neutralization parameters, such as concentration and reaction time, a sodium carbonate/bicarbonate buffer solution was prepared to simulate the lake water. The solution pH was adjusted to the same value as the lake

water. Two milliliters of the prepared carbonate/bicarbonate buffer solution was mixed with 0.5, 2, or 6 mL 0.1 M $CaCl_2$ or $MgCl_2$ in separate 15-mL centrifuge tubes to examine the pH reduction and the solid phases formed during alkalinity neutralization. The suspension after adding $CaCl_2$ or $MgCl_2$ was taken out by drop pipet and transferred on the XRD glass slide. The XRD analysis of solid phases was then performed after overnight drying. A NaCl solution was used as control. After determining the optimal concentration of the chemicals in reducing the pH, the reaction time (30 seconds, 5, 10, 30 minutes) was evaluated. Visual MINTEQ 3.1 was used to predict pH reduction from the mineral formation.

2.5.2. Alkalinity neutralization of bauxite residue supernatant by Ca^{2+} and Mg^{2+}

The optimal dosage (0.1 M, 6 mL) obtained from lake water simulant described previously were then used for the bauxite residue liquid phase neutralization mechanisms studies. Three grams of bauxite residues were centrifuged at 3000 xg (m/s^2) for 5 minutes in a 15-mL centrifuge tube. Only the supernatants were collected and treated with 6 mL 0.1 M $CaCl_2$ and $MgCl_2$. After three times DI water washing, the precipitates were harvested for XRD analysis.

2.5.3. Alkalinity neutralization of bauxite residues

To evaluate the efficiency of $CaCl_2$, $FeCl_3$, H_2SO_4, and NaH_2PO_4 in reducing the pH of the bauxite residues. The bauxite residue was mixed with a solution of the chemicals at a 1:2 ratio (wet slurry mass: liquid volume) in a 15-mL centrifuge tube. Three concentrations of each chemical were selected to determine the concentration needed to reduce the pH to between 7 and 8. Except for the $CaCl_2$ solutions, all other

three chemicals were dissolved in the 0.1 M NaCl to maintain high ionic strength similar to the original bauxite residue liquor. Three replications were performed for each treatment. The centrifuge tubes were mixed by a vortex mixer at 2095 xg (m/s^2) for 10 seconds and then shaken on a reciprocal shaker overnight. The supernatant pH for all samples was measured after the solid-liquid separation by gravity settling.

2.5.4. Settling performance of bauxite residues

2.5.4.1. Settling ratio

Residue settling performance was evaluated by the settling ratio, which was defined as[36]:

$$Settling\ ratio\ (\%) = \frac{Vi - Vt}{Vi} \times 100\%$$

where *Vi* was the initial volume of the slurry in a container and *Vt* was the settled volume of the sediment at time t.

2.5.4.2. Settling enhancement with surfactants and polymers

As will be seen in the result section, reducing the pH of the residue would not improve settling. The following five solutions were prepared to test their effectiveness in improving the settling of the pH-reduced residues: 2 g/L cationic, neutral, and anionic polyacrylamide (PAM) and 0.5 g/L sodium dodecyl sulfate (SDS) and benzyl tetradecyl dimethyl ammonium chloride (BDTDA) stock solutions. All solutions were prepared in a 0.1 M NaCl solution and then shaking 24 hours before use. All the chemicals were analytical grade. Three grams of wet bauxite residues slurries were reacted with certain volume of $CaCl_2$, $FeCl_3$, H_2SO_4 or NaH_2PO_4 in 15 mL centrifuge tubes overnight first to

neutralize the alkalinity. The volume of neutralization solution added was calculated from subtracting the settling solutions volume needed later. For example, 1.5 mL PAM solution was needed for 1 g/kg (PAM/bauxite residues), so 4.5 mL chemical solutions were required in order to keep the final slurry mass to liquid volume ratio equal to 1:2. The pH after different neutralization volumes were inspected and show the differences were not significant (<0.5). After shaking, settling solutions were added into the tubes. For SDS and BDTDA, tubes were mixed, shaken overnight again, vibrated by Vortex mixer, and then allowed to settle under gravity. To prevent floc breakage, tubes were only gently flipped upside-down several times for PAM adding samples.

The settling volumes at 1 hour and 24 hours were measured, before and after alkalinity neutralization treatments and PAM addition, to determine the effects of charge types of PAM and electrolytes by a two-way ANOVA[37]. Post hoc comparisons were performed using LSD with Bonferroni correction and all hypothesis tests were two-sided and tested at an alpha level of 0.05.

3. RESULTS AND DISCUSSIONS

3.1. Mineral composition and transformation of bauxite residue during storage

3.1.1. Physical and chemical properties

The bauxite residues were characterized by high-water content, high pH, and high salinity (Table 3-1). Among the 54 samples analyzed, more than 90% of the samples had water contents greater than 100%. Except for two specimens, all other samples had pH > 10; more than 70% of the samples had EC readings greater than 2 mS/cm. For the land samples, the average water content (146%) of the top sections were slightly greater than that of the bottom sections (128%), while the pH (10.3) and EC (2.05 mS/cm) of the top section were lower than those of the bottom sections (pH: 11.8, EC: 3.39 mS/cm). High water contents of top section could be explained by the effect of precipitation. Rainwater might have leached ions downward and decreased pH and EC of the top sections. Less leaching of the bottom section could occur due to the low hydraulic conductivity, one major obstacle of bauxite residues[3], impeding the vertical flow from top section. Lower pH and EC of the stored bauxite residue compared to fresh bauxite residue has also been observed in previous studies[38]. Significant reduction of pH from 12 to about 10 by rinsing with H_2O was reported. It was pointed out that the stable pH after increasing washing times was due to the carbonate buffer effect[36]. Carbonation from atmospheric CO_2 was confirmed to reduce the pH from 12.3 to 9.3 up to a depth of 1.2 m in the storage cell after 35 years storage[39]. Thus, the carbonate/bicarbonate buffer was believed to account for the alkaline pH in the liquid phase.

The mineral compositions at different locations were very similar horizontally, the details of mineral compositions will be discussed later. Except for some outliers, such as 1B1 bottom section or 1C1 top section, the land area can be regarded as uniform horizontally based on the water content, pH, EC and mineral compositions (Table 3-2).

The water contents and pH of bauxite residue in the lake area had similar tendency as the land samples, but there was no apparent separation in the EC values between top and bottom sections. Inconsistent results of EC might be due to the higher water content, thus more liquid (major source of electrolytes) would be taken when measuring the EC.

Table 3-1 Average water content, pH, EC and mineralogical results of top or bottom section in land and lake zone

Zone		Water content		pH		EC		Fe-oxide minerals[a]		Al-oxide minerals[b]	
		(%)				mS cm-1		(%)		(%)	
		Top	Bottom	Top	Bottom	Top	Bottom	Top	Bottom	Top	Bottom
Land	Mean	146	128	10.3	11.8	2.05	3.39	52.9	16.0	18.9	11.0
(N = 18)	SD[c]	30	26	1.8	0.4	1.05	0.61	15.5	16.0	18.9	11.0
Lake	Mean	227	128	10.5	11.5	2.53	2.14	14.2	59.8	45.8	13.1
(N = 9)	SD	96	36	0.35	0.50	0.48	0.92	7.3	20.9	16.9	3.90

[a]Fe-oxide minerals included hematite (Fe2O3) and goethite (FeOOH).
[b]Al-oxide minerals included boehmite (AlOOH), gibbsite, bayerite, and nordstrandite [Al(OH)3].
[c]Standard deviation

Table 3-2 Water content, pH and EC of all top and bottom sections.

Zone		Water content		pH		EC		Fe-oxide minerals		Al-oxide minerals	
		(%)				mS cm-1		(%)		(%)	
	Sample	Top	Bottom	Top	Bottom	Top	Bottom	Top	Bottom	Top	Bottom
Land	1A1	145	151**	10.2	11.7	1.44*	2.74***	56.3	70.2	15.4*	10.2
	1A2	157	142*	10.7	12.0	1.06**	3.41	59.9	69.9	15.4*	10.8
	1A3	159	138	7.2***	12.1	0.75***	3.52	21.9***	65.4	33.3***	11.7
	1B1	172**	38***	11.9***	12.2	3.44***	4.00***	62.8*	5.7***	18.3	16.7***
	1B2	100***	152**	9.9	12.3	2.31	4.06***	48.9	70.6	21.7	8.6**
	1B3	154	129	9.3*	11.9	2.13	2.45***	66.6***	72.0	11.1***	9.3*
	1C1	134	133	7.1***	11.8	0.89***	3.14	23.9***	69.3	25.6***	9.1*

Table 3-2 Continued

Zone		Water content		pH		EC		Fe-oxide minerals		Al-oxide minerals	
		(%)				mS cm-1		(%)		(%)	
	Sample	Top	Bottom	Top	Bottom	Top	Bottom	Top	Bottom	Top	Bottom
Land	1C2	115***	138	7.2***	11.7	0.67***	2.88**	22.1***	67.4	21.9	12.7*
	1C3	87***	148**	8.4***	11.8	0.89*	3.22	43.0*	67.0	21.7	12.2*
	2A1	167**	136	11.6**	12.2***	2.63*	4.47***	59.8	74.8	18.6	9.7*
	2A2	118***	124	10.1	11.2***	2.24	2.97*	55.8	79.9**	19.8	6.1***
	2A3	192***	124	11.5**	10.9***	2.34	3.12	64.9**	76.5*	15.3*	7.5***
	2B1	123**	131	11.1	11.9	3.14***	3.70*	65.8**	74.3	16.2	10.5
	2B2	154	90***	10.3	10.9***	1.29**	2.28***	60.0	65.5	13.8***	13.0**

Table 3-2 Continued

Zone		Water content		pH		EC		Fe-oxide minerals		Al-oxide minerals	
		(%)				mS cm-1		(%)		(%)	
	Sample	Top	Bottom	Top	Bottom	Top	Bottom	Top	Bottom	Top	Bottom
Land	2B3	198***	127	11.9***	12.0	3.08***	3.82**	67.9***	70.8	13.7***	15.2***
	2C1	163**	130	11.8**	12.0	3.23***	3.72*	54.3	73.9	20.4	12.4*
	2C2	127**	132	12.1***	12.1**	4.03***	4.23***	50.9	76.0*	27.0***	11.7
	2C3	155	145*	12.1***	12.0	1.31**	3.26	67.9***	64.9	10.2***	9.8*
Lake	3-1	325*	143	10.6	10.3***	2.48	1.49	26.1***	67.2	52.2	15.8
	3-2	273	111	10.7	11.6	2.13*	1.58	14.7	56.8	53.0	6.8**
	3-3	115**	133	10.3	11.6	2.19	1.62	7.6*	71.1	57.6	17.0*

Table 3-2 Continued

Zone		Water content		pH		EC		Fe-oxide minerals		Al-oxide minerals	
		(%)				mS cm-1		(%)		(%)	
	Sample	Top	Bottom	Top	Bottom	Top	Bottom	Top	Bottom	Top	Bottom
Lake	4-1	322*	42***	10.4	11.7	2.04*	2.20	17.4	5.6***	62.4*	10.4
	4-2	266	137	10.3	11.7	2.94*	2.83	18.0	73.1	47.0	11.9
	4-3	242	129	10.3	11.5	3.14**	1.78	20.4*	62.8	47.1	19.7**
	5-1	277	137	10.7	11.7	2.70	1.94	10.5	65.4	48.9	10.9
	5-2	185	164*	11.2***	12.1**	3.17**	4.30***	11.5	70.3	39.9	11.9
	5-3	41***	159*	10.0**	11.3	1.95**	1.49	1.9***	66.1	4.3***	13.7

Note. Confidence interval was calculated for either land or lake zone. No asterisk denoted nonsignificant; * denoted significant at the 95% confidence level; ** denoted significant at the 99% confidence level; *** denoted significant at the 99.9% confidence level

The water samples collected in three lake zones had similar chemistry: high salinity of EC reading of 12.4-12.8 (mS/cm), and high pH of 9.8. The dominant cation was Na^+ with a concentration between 3800 to 3900 mg/L. The dominant anions are bicarbonate and carbonate (Table 3-3). As sodium hydroxide was utilized to extract the aluminum in the Bayer process, it was the initial source of sodium and alkaline pH of the bauxite residue slurry[4]. Hydroxide ions were neutralized over time by atmospheric carbon dioxide, which formed carbonate and bicarbonate buffer ions during disposal[14]. Carbonate ions could further react with calcium and magnesium ions to form calcite or magnesium carbonate minerals and cause the low concentration of both cations in the lake water.

$$CO_2 + OH^- \leftrightharpoons HCO_3^- \quad (3\text{-}1)$$

$$HCO_3^- + OH^- \leftrightharpoons \mathrm{CO_3^{2-}} + \mathrm{H_2O} \quad (3\text{-}2)$$

$$Ca^{2+} + \mathrm{CO_3^{2-}} \leftrightharpoons \mathrm{CaCO_{3(s)}} \quad (3\text{-}3)$$

Two major groups of bauxite residue samples—Fe-oxide and Al-oxide dominated—were identified based on mineralogical compositions. Rapid titration curve for both Fe-oxide and Al-oxide dominated samples with or without lake water, confirmed the existence of the carbonate/bicarbonate not only in the lake water but also in the pore waters (Figure 3-1). The final pH of MINTEQ simulation based on the carbonate concentration in Table 3-3 matched well with the Fe-oxide dominated bauxite residue and the curve transition point difference could be attributed to the high proportion of bicarbonate in the liquid phase of bauxite residue. The MINTEQ

prediction deviated the titration curve of the Al-oxide dominated bauxite residue after adding 20 mL titrant. The deviation was likely caused by the dissolution of solids. After 24 hours, the pH reverted to about 6.6, indicating the dissolution of sodium aluminum silicate between pH 6.7 to 8.7 (Equation (3-4))[12]. For 20 g Fe-oxide-dominated bauxite residue, about 20 mL 0.1 M H_2SO_4 was needed to reduce pH to 6, corresponding acid neutralization capacity of 0.2 mEq/g bauxite residue. This acid neutralization capacity was significantly lower than the value of 1.2 mEq/g reported in a previous study because the atmospheric CO_2 consumed the alkaline species in the pore water during storage. The narrow horizontal buffer region in titration curve as the result of the dissolution of sodalite, tricalcium aluminate, calcite, or other alkaline compounds after 20 years storage was proposed by Kong et al[40]. The transformation of tricalcium aluminate to calcite in the disposal pond exposed to atmospheric CO_2 was reported[14]; thus, the lack of tricalcium aluminate (buffer in pH range 8.7 to 9.9, Equation (3-5)) in our bauxite residue might also decrease the acid neutralization capacity[12].

$$NaAlSiO_{4(s)} + 4H^+ \leftrightharpoons Na^+ + Al^{3+} + Si(OH)_4 \quad (3\text{-}4)$$

$$Ca_3Al_2O_{6(s)} + 12H^+ \leftrightharpoons 3Ca^{2+} + 2Al^{3+} + 6H_2O \quad (3\text{-}5)$$

Table 3-3 Chemical compositions and properties of the bauxite residue storage lake zones

Sample	Ca	Mg	Na	K	CO_3	HCO_3	SO_4	Cl	pH	EC
	mg/L									mS/cm
Zone 3	3	4	3941	58	1268	7448	598	611	9.81	12.5
Zone 4	2	1	3864	57	1188	7098	595	613	9.84	12.8
Zone 5	2	1	3790	57	1219	7275	592	616	9.85	12.4

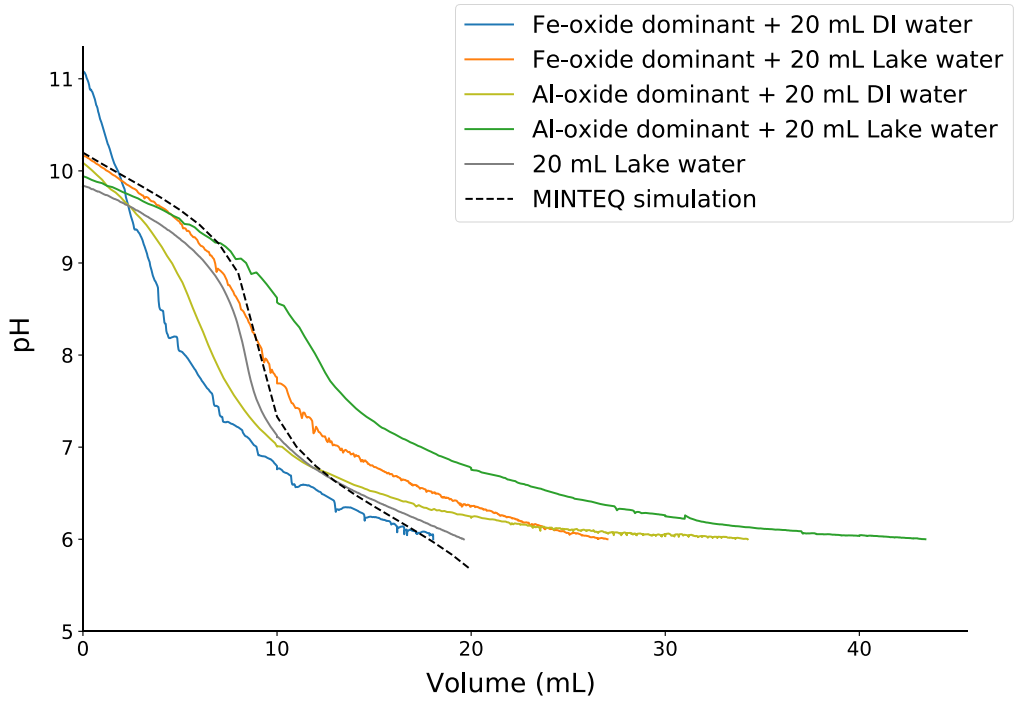

Figure 3-1 Rapid titration with 0.1 M H_2SO_4 of 20 g Fe-oxide, Al-oxide dominated bauxite residue with 20 mL DI or lake water and MINTEQ simulation of 0.14 M carbonate solution after adjusting the starting pH~10

3.1.2. Mineral compositions and sample merge

Major minerals in bauxite residues were Fe-oxides (hematite, goethite), Al-oxides (boehmite, gibbsite, bayerite, nordstrandite), calcite, and quartz. The mineral compositions would be discussed in next section in detail (3.1.3). The k-means algorithm was used to group the samples based on their similarity of mineral compositions. Elbow method was applied to determine the optimal number of clusters. Distances change from 3 to 5 are all tending to converge. Silhouette coefficient method was employed to assist in obtaining the optimal k. Maximum appears at k =3, and therefore an optimal number of clusters of three was chosen in group the bauxite residue samples based on mineral composition (Figure 3-2).

Three groups of samples were (1) Fe-oxide dominated bauxite residue; (2) Al-oxide dominated bauxite residue and (3) non bauxite residue soil or sediment. The spatial distribution of mineral groups was illustrated in Figure 3-3. The small portion of the soil or sediment was likely due to the original marine sediment before the disposal pond was built or due to the sediment transport in previous residue management operation. The few soil or sediment samples did not represent the bauxite residue well. To represent the Fe-oxide dominated and Al-oxide dominated bauxite residues for the follow alkalinity neutralization and settling experiments, one of the 45-cm-long section sample from five different cores under the lake area were combined to form one Fe-oxide dominated bauxite residue and the other five were combined to form one Al-oxide dominated bauxite residue.

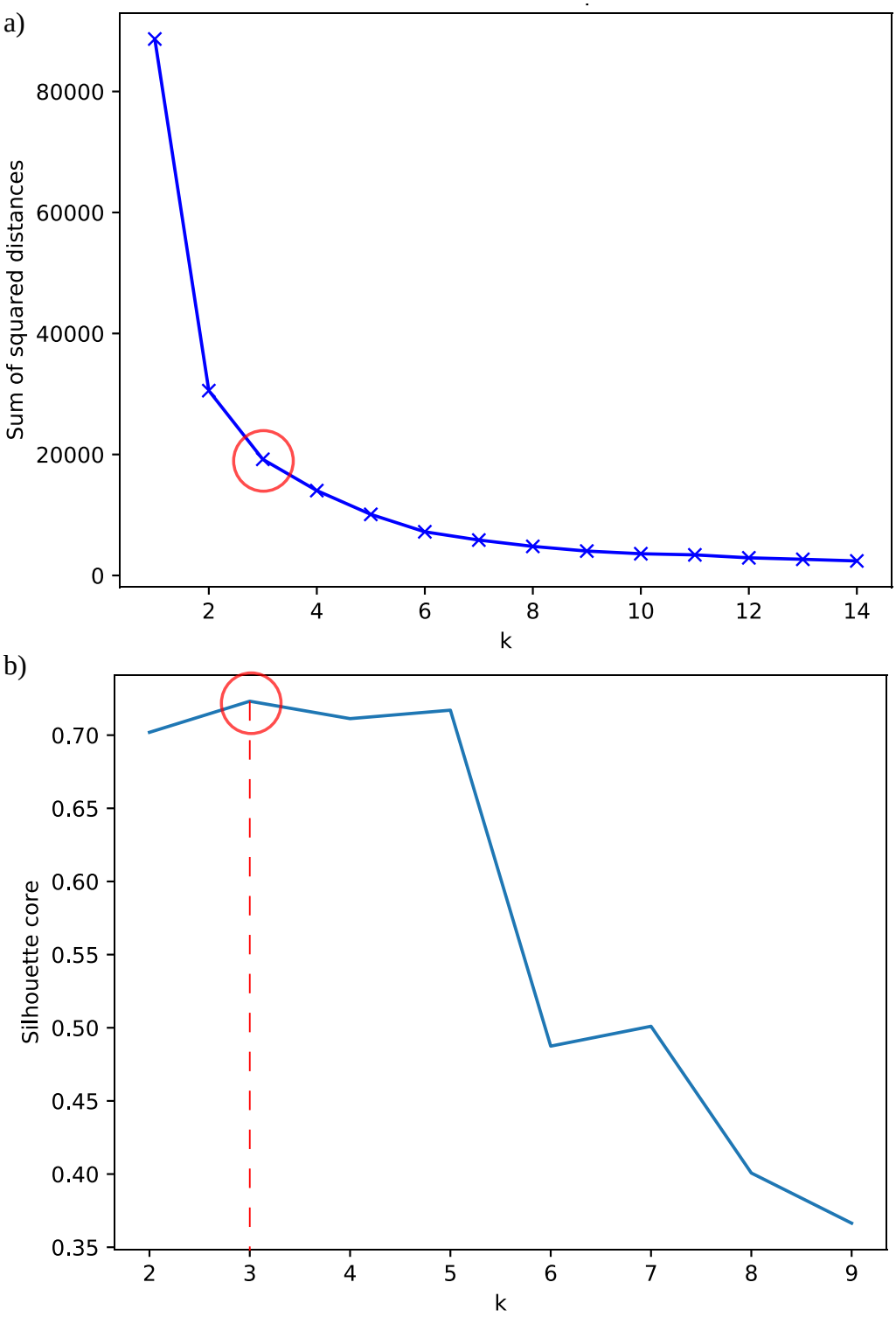

Figure 3-2 (a) Elbow and (b) silhouette coefficient method for optimal cluster numbers. Both methods suggested that three (turning point and peak) was the optimal.

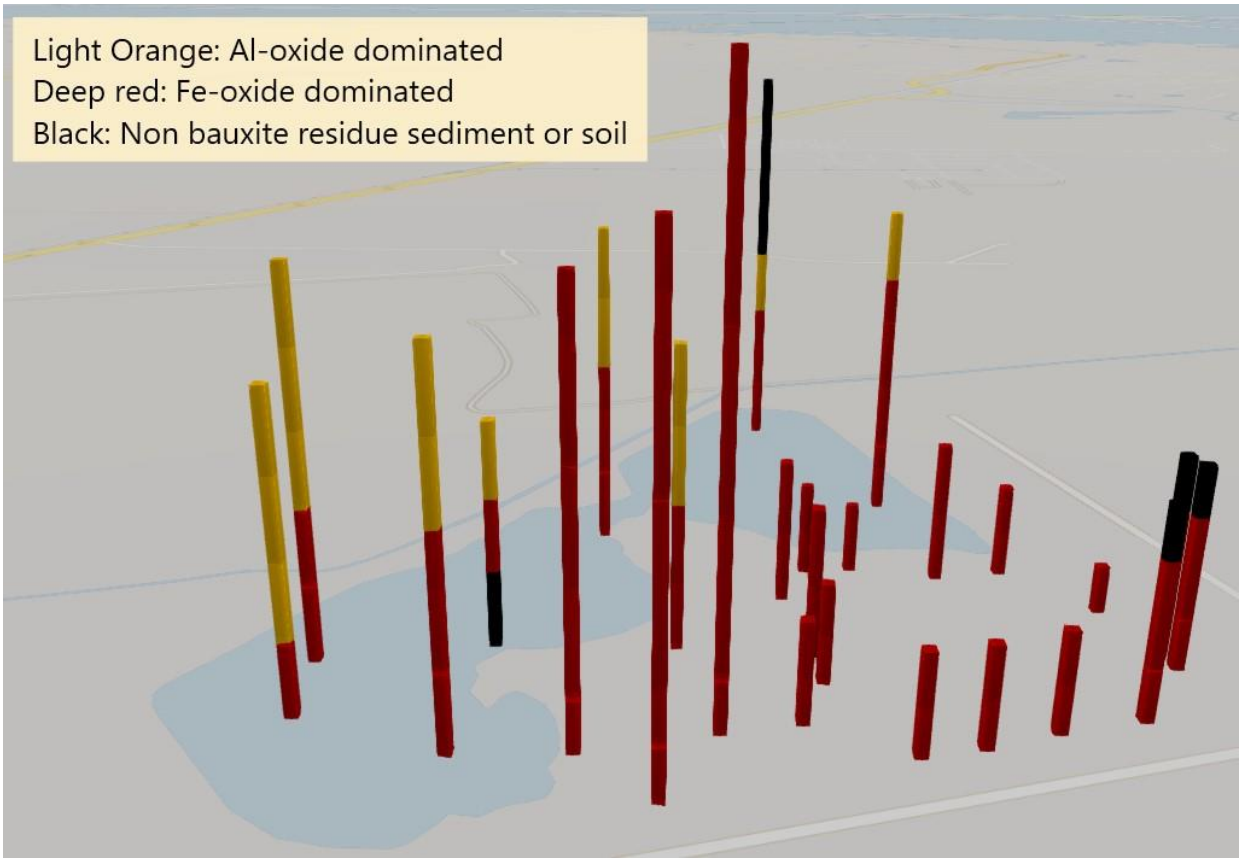

Figure 3-3 Distribution of different groups of samples in the disposal area (top of each bar was the disposal area ground surface)

3.1.3. Mineralogical characterization of Fe-oxide and Al-oxide dominated bauxite residue

Major mineral phases in Fe-oxide dominated bauxite residue were hematite, goethite, boehmite, bayerite, and calcite, while bayerite, nordstrandite, gibbsite, bayerite, hematite, and goethite dominate in Al-oxide dominated bauxite residue (Table 3-4). It was noteworthy that the aluminum oxides were dominant in the section of the top lake residue, which was uncommon in the typical bauxite residues. Common Bayer process characteristic solids (BPCSs), such as sodalite, cancrinite, and tricalcium aluminate[3], were not observed on the XRD pattern (Figure 3-4) in current study.

FTIR of Fe-oxide dominated bauxite residue and reference minerals (Figure 3-5) supported the mineral identification from XRD. The IR bands at around 1420, 870, 710 cm^{-1} corresponded to calcite and 3097 cm^{-1} to goethite, respectively. The weak peak at around 960 cm^{-1} matched well with the pure hematite, and the intense, broad band at around 3400 cm^{-1} was believed to be due to water molecules. Characteristic boehmite peaks at 3287, 3097, 1149, 1070 cm^{-1} were observed and agreed well with a previous study[41]. For the Al-oxide dominated group, besides calcite and broad water band, the peaks at 3617, 3519, 3424, 3362 and 1011 cm^{-1} supported the presence of gibbsite (Figure 3-6). In line with previous studies, SEM images of both groups (Figure 3-7) revealed the bauxite residue contained aggregates composed of fine particles[21, 42].

Table 3-4 Mineral quantitative analysis of merged Fe-oxide and Al-oxide dominated bauxite residue by Rietveld refinement

Mineral phase	Fe-oxide dominated (wt%)	Al-oxide dominated (wt%)
Hematite	40.5	14.7
Goethite	23.3	6.3
Total Fe-oxide	63.8	21.0
Boehmite	9.3	2.3
Gibbsite	1.9	21.7
Bayerite	4.1	7.8
Nordstrandite	1.2	24.1
Total Al-oxide	16.5	55.9
Calcite	7.0	17.0
Trona	2.7	0.2
Thermonatrite	8.7	4.0
Rutile	0.7	0.9
Quartz	0.5	0.9

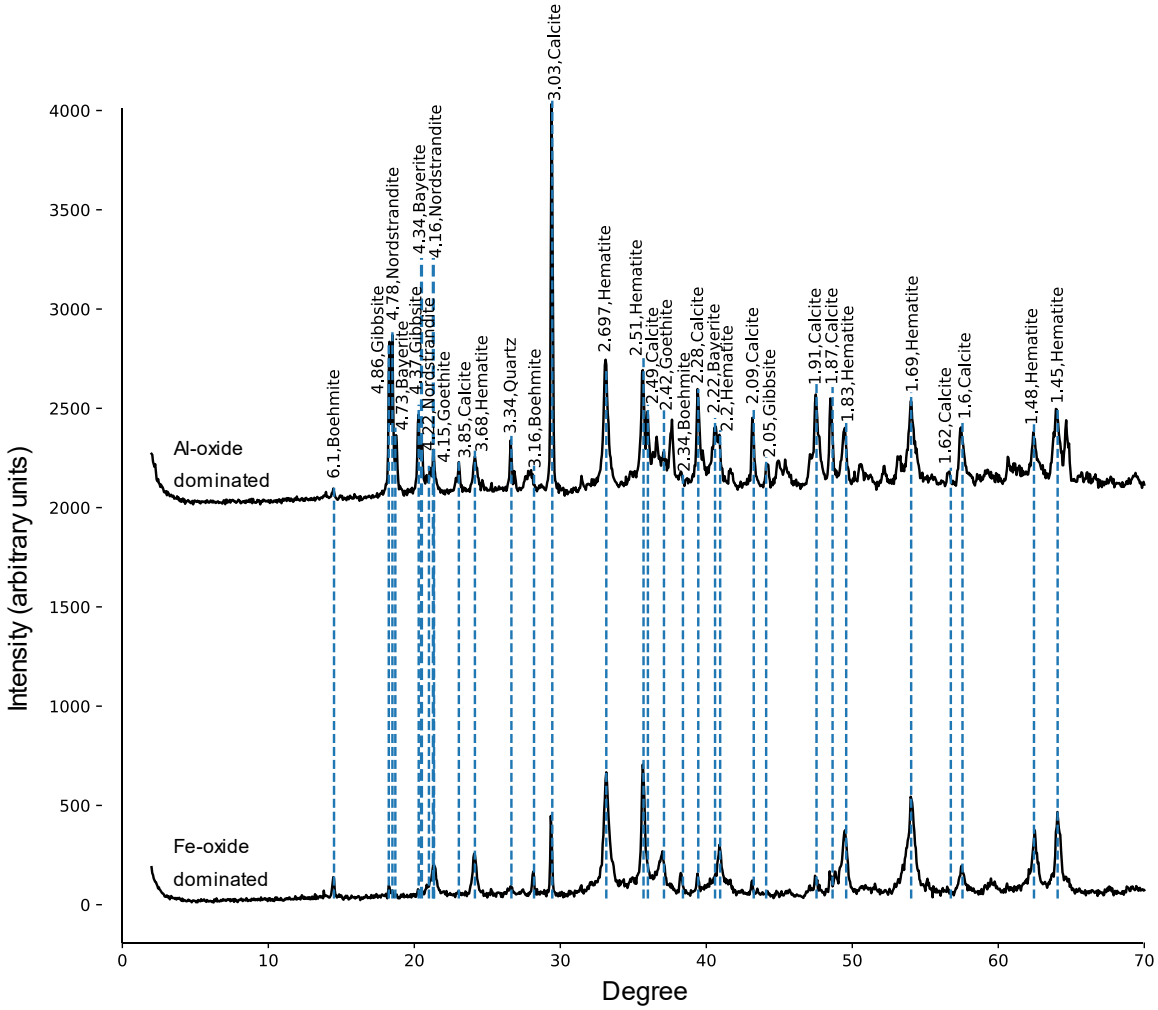

Figure 3-4 XRD pattern of merged Fe-oxide and Al-oxide dominated bauxite residue

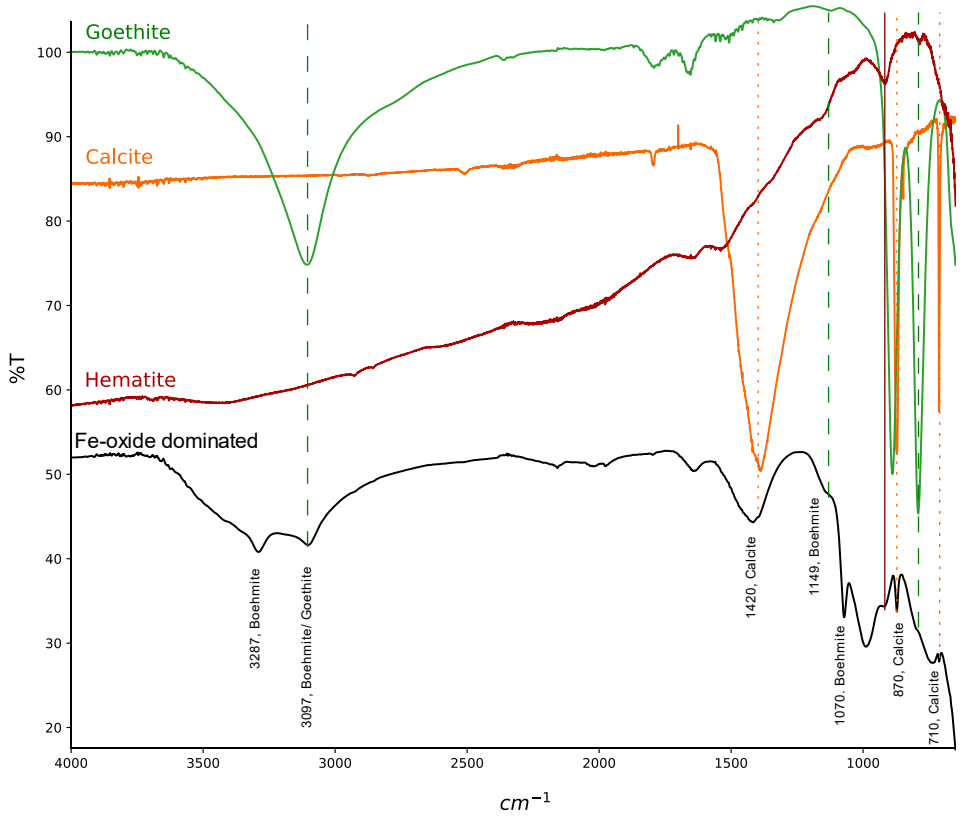

Figure 3-5 FTIR of Fe-oxide dominated bauxite residue and reference minerals

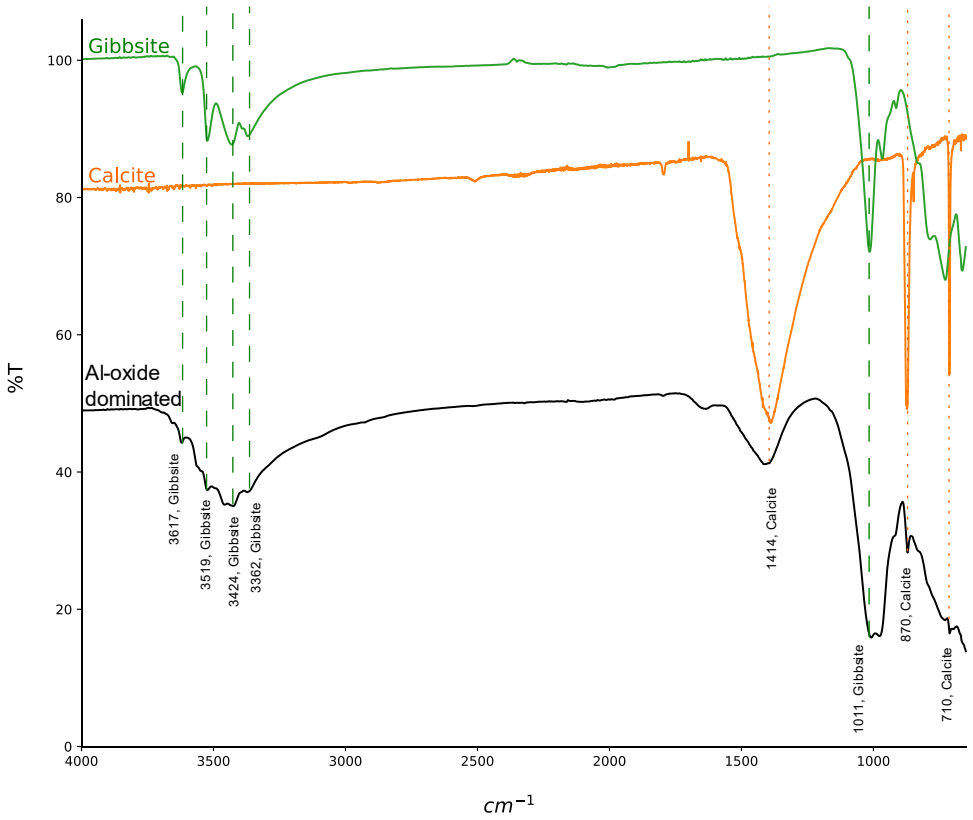

Figure 3-6 FTIR of Al-oxide dominated bauxite residue and reference minerals

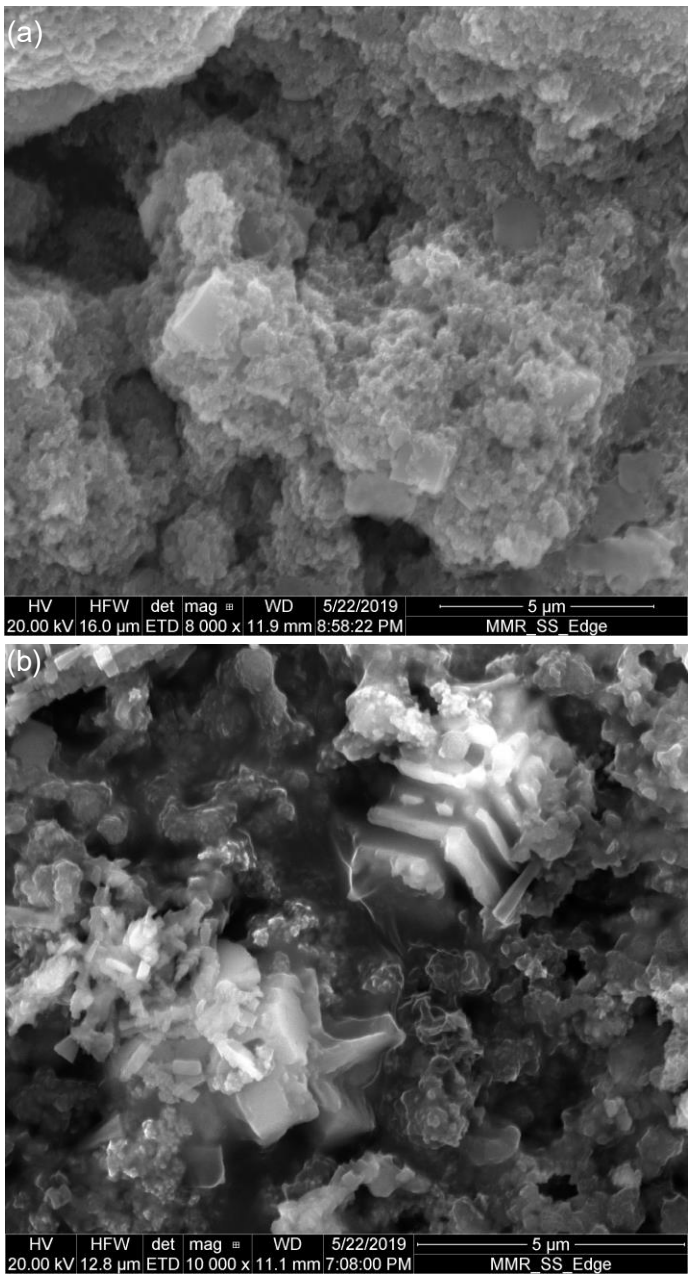

Figure 3-7 SEM image of (a) Fe-oxide dominated bauxite residue and (b) Al-oxide dominated bauxite residue

3.1.4. Mineral transformation during storage

3.1.4.1. Fe-oxide dominated bauxite residue

Bauxite residue in this disposal facility has been studied in the past and it is known that the bauxite ore was originated from Jamaica[12]. The iron oxide in the ore was mainly hematite. Mineral composition confirmed that Jamaican bauxite consists of mainly gibbsite, boehmite, hematite, and goethite with minor amount of titanium oxide and silicon oxide[43]. The scarcity of aluminosilicate clay minerals in the Jamaican bauxite could explain the lack of sodalite and cancrinite, the common Bayer process characteristic solids (BPCSs), in current samples. A less than 1% Bayer-sodalite in Jamaican bauxite residue was reported from previous research[44]. Transformation of another common BPCSs, tricalcium aluminate, to calcite exposed to atmospheric CO_2 during storage was mentioned before and was believed to be one possible source of the calcite in current samples. Interestingly, only trace amounts of gibbsite, the most common aluminum oxide mineral in bauxite residue, was presented in the Fe-oxide dominated residue. It could be an indication of the transformation of gibbsite during storage.

Hydrothermal simulation of the long-term weathering of bauxite residue indicated that (1) pH and EC of the residues decreased over time; (2) sodalite, cancrinite, and tricalcium aluminate either dissolved or transformed to calcite; (3) boehmite, goethite, hematite, and calcite would be the stable mineral phases after long-term weathering[45]. The simulation was in good agreement with the mineral compositions of the Fe-oxide dominated bauxite residue, but it failed to predict bayerite formation.

Unsuccessful prediction of bayerite formation could be the result of high temperature and pressure used in the hydrothermal simulation experiment. Bayerite precipitation under alkaline and room temperature conditions has been reported in several studies[46-48]. It was confirmed that gibbsite may transform to boehmite or bayerite during the disposal in strong caustic environment[49].

3.1.4.2. Minerals in surface crust in land area and Al-oxide dominated bauxite residue

Nordstrandite, bayerite and calcite were found in the surface crust of land area (Figure 3-8 and Figure 3-9). Absence of hematite and goethite, the major components in current bauxite residue, in the crust suggested that crystallization and precipitation of the aluminum hydroxide and calcite occurred in the crust during the storage. Rapid bayerite formation under alkaline condition and transformation to nordstrandite during aging under intermediate to high pH range were suggested by earlier researchers[47]. Formation of nordstrandite in current study could be attributed to two possible mechanisms: (1) local pH reduction driven by calcite formation; (2) preferred crystallization induced by high sodium concentration under evaporation condition. With the first mechanism, when external calcium ions were introduced into the residue, calcite precipitation consumed the carbonate ions in the solution, reducing the pH and promoting nordstrandite formation[50]. This mechanism resembles common natural condition when nordstrandite occurs with presence of limestone (calcium carbonate minerals), which provides a neutral to alkaline pH condition. The $Al(OH)_3$ phase diagram with NaCl concentration

and pH as variables suggested that a higher NaCl concentration would prompt the formation of nordstrandite[51]. A similar conclusion was reached by identifying natural nordstrandite in an unique Na-rich condition with pH > 7[52]. However, contrary to other studies, no carbonate minerals present in this environment. Increasing salt concentrations in solution due to evaporation might result in the formation of bayerite and norstrandite in addition to calcite in the surface crust of land area. A similar hard crust, composed of various carbonate minerals, was discovered under alkaline and high electrolyte concentration in a long-term Hanford site storage tank recently[53]. Evaporation and further capillary rise of underneath liquid were believed to be the main reason for the formation of the hard crust on the surface. The aluminum hydroxide and calcite cemented each other to the formation of a hard surface crust in current study.

The top bauxite residue layer of lake area was identified as Al-oxide dominated bauxite residue. Gibbsite, bayerite, and nordstrandite were the major aluminum oxide mineral phases. Formation of bayerite and nordstrandite might occur with above-described mechanism: pH reduction by carbonization and high salt concentration promoted the phase transformation. It is noteworthy that gibbsite only occurred in the top residue layer of lake area but not in the surface crust of the land area. This might be due to the lower pH of the lake water, which could prevent gibbsite from dissolving and further transforming in the lake. The gibbsite in “fresh” bauxite residue was discarded into the lake and remained stable during storage. However, an *in situ* transformation alone cannot account for the higher total percentage aluminum oxide content in the top layer. It was likely that the diffusion of aluminate from bottom layer induced

precipitation of aluminum minerals in the upper layer of the residue when the pH was lower than those below. In the lake, pH was reduced to 9.8 by atmospheric CO_2 allowing aluminum hydroxide to precipitate, which reduced local aluminum concentration in the liquid and improved the migration of aluminum ions from bottom.

$$Al(OH)_{4\,(aq)}^{-} + H^{+} \leftrightharpoons Al(OH)_{3\,(s)} + H_2O \quad (3\text{-}6)$$

$$Al(OH)_{3\,(s)} \leftrightharpoons AlOOH_{(s)} + H_2O \quad (3\text{-}7)$$

Figure 3-8 Surface crust formed on the top of land area

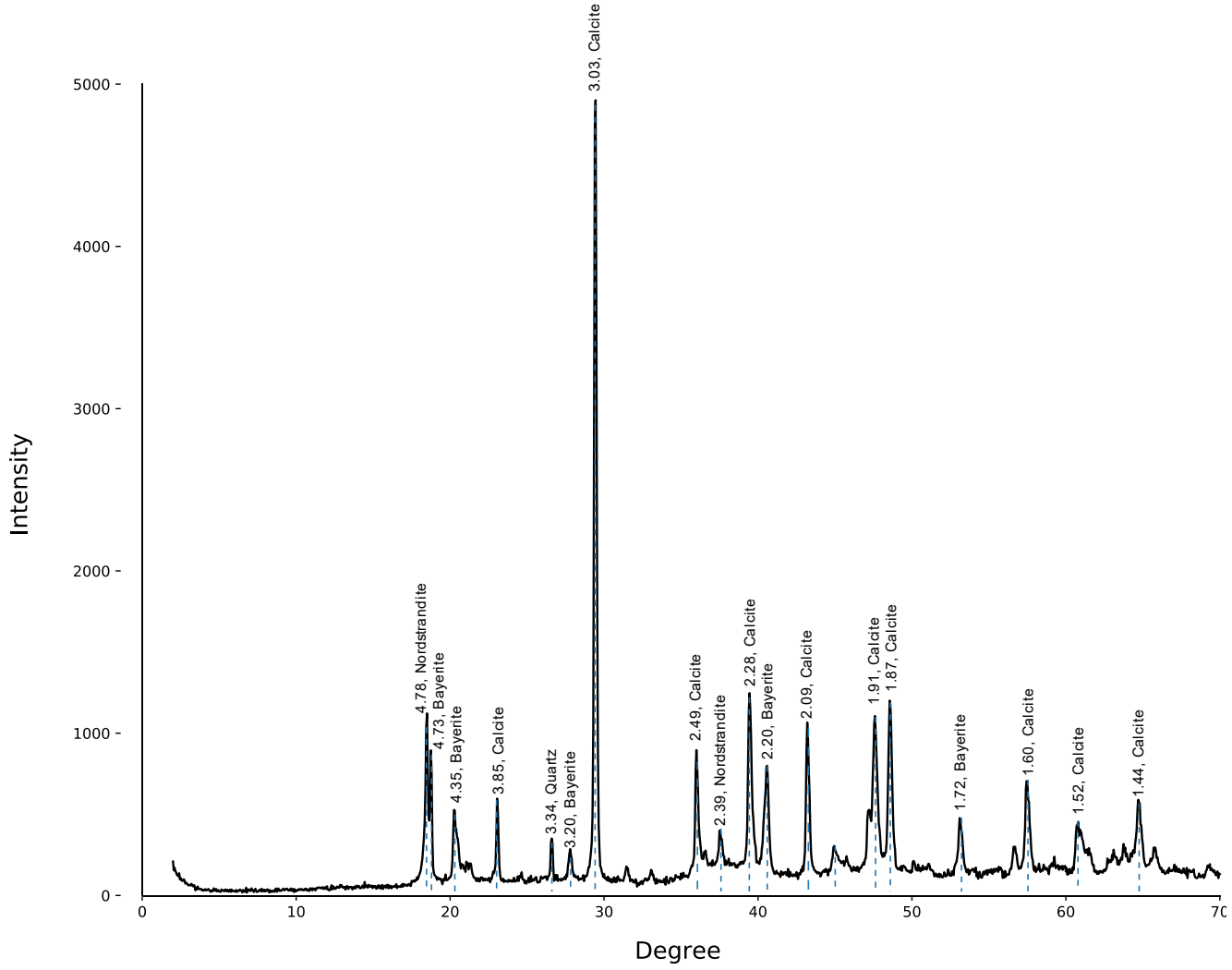

Figure 3-9 XRD pattern of the surface crust found on the land area

3.2. Alkalinity neutralization and settling performance of bauxite residue

3.2.1. Alkalinity neutralization of bauxite residues

3.2.1.1. Carbonate formation in bauxite residue liquid simulant when alkalinity was neutralized with Ca^{2+} and Mg^{2+}

Sodium carbonate and sodium bicarbonate with a total concentration equal to 0.1 M were prepared to simulate the liquid phase of bauxite residues. Based on the pH of the Fe-oxide dominated bauxite residue pore water, the ratio of carbonate and bicarbonate was adjusted. Two salts, $CaCl_2$ and $MgCl_2$, were used as calcium and magnesium sources for alkalinity neutralization.

The pH (Figure 3-10) of carbonate/bicarbonate simulant reacted with different amounts of 0.1 M $CaCl_2$ and $MgCl_2$ solution indicated that both treatments could reduce pH, and calcium was more effective than magnesium in reducing pH. The neutralization reactions were fast (less than 1 min) for both reactions (Figure 3-11).

The measured pH of carbonate/bicarbonate simulant during neutralization by Ca^{2+} matched well with the simulation using Visual MINTEQ (Table 3-5). The simulated pH had large deviations for the $MgCl_2$ neutralization. Inaccurate results were likely due to the incorrect selection of mineral phases in MINTEQ. In current simulation, MINTEQ predicted calcite and magnesite as the precipitate in the $CaCl_2$ and $MgCl_2$ treatments, respectively. However, no substantial precipitate was observed when $MgCl_2$ was added to the carbonate/bicarbonate simulant (Figure 3-12). Amorphous phases, which are not most thermodynamically stable solid, may form in the solution leading to the decrease of pH.

The XRD analysis indicated that the calcite, vaterite, and halite (Figure 3-13) precipitated when $CaCl_2$ was added to the carbonate/bicarbonate simulant. When titrated with $MgCl_2$, halite and hydrated magnesium chloride were the dominant crystalline phases. The small hump at 2-theta from 20-40 degrees indicated the presence of amorphous phases.

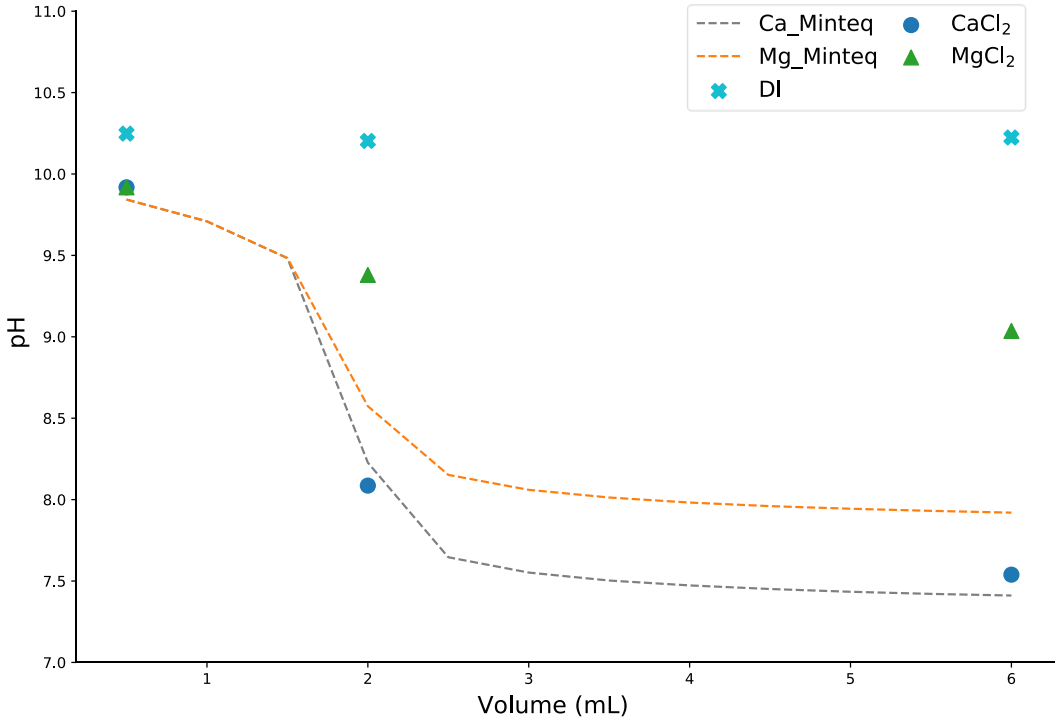

Figure 3-10 The pH of 2 mL carbonate/bicarbonate simulant reacted with 0.5, 2, and 6 mL DI water or 0.1 M $CaCl_2$ or $MgCl_2$

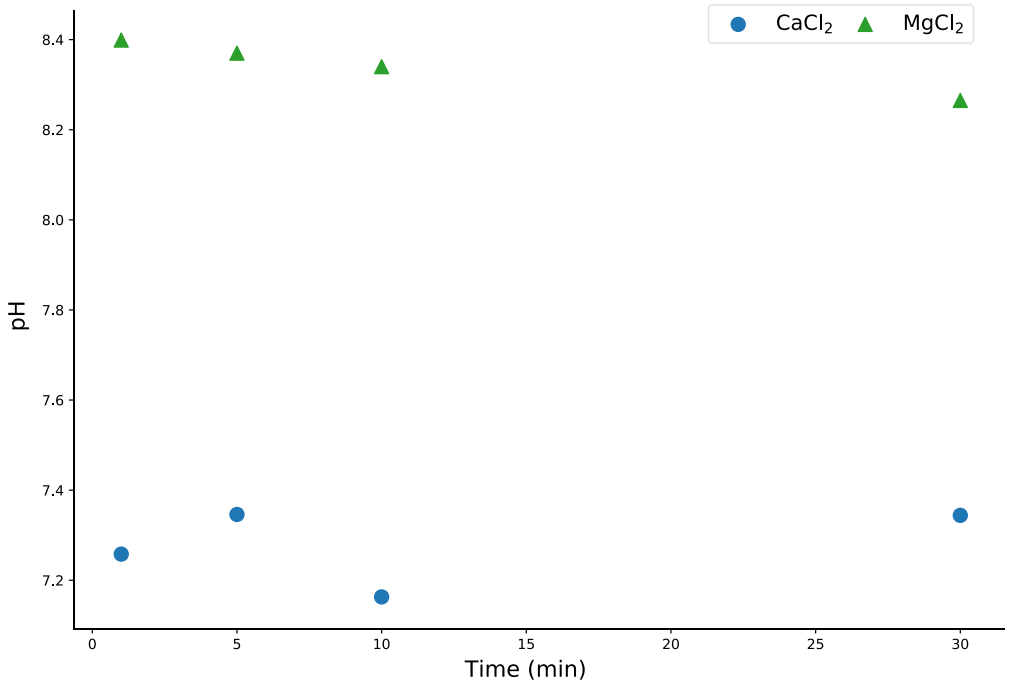

Figure 3-11 The pH of 2 mL carbonate/bicarbonate simulant reacted with 6 mL 0.1 M $CaCl_2$ and $MgCl_2$ for 0.5 to 30 min

Table 3-5 Measured and MINTEQ simulated pH of 2mL carbonate/bicarbonate simulant after adding 0.1 M $CaCl_2$ and $MgCl_2$

Treatment		Volume (mL)		
		0.5	**2**	**6**
$CaCl_2$	Measured pH	9.92	8.09	7.54
	MINTEQ	9.76	8.31	7.47
$MgCl_2$	Measured pH	9.92	9.38	9.04
	MINTEQ	9.76	8.66	7.99

a) 0.1 M $CaCl_2$

2 mL 6 mL

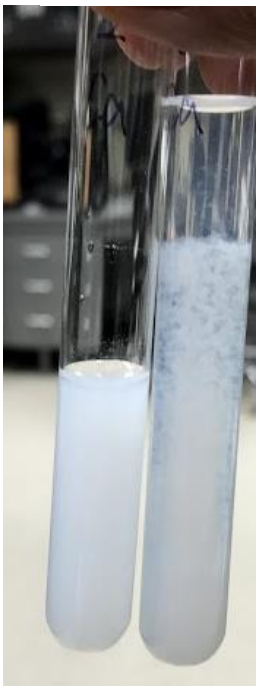

b) 0.1 M $MgCl_2$

2 mL 6 mL

Figure 3-12 Precipitates of 2 mL carbonate/bicarbonate simulant after adding 2 or 6 mL of 0.1 M (a) $CaCl_2$ and (b) $MgCl_2$

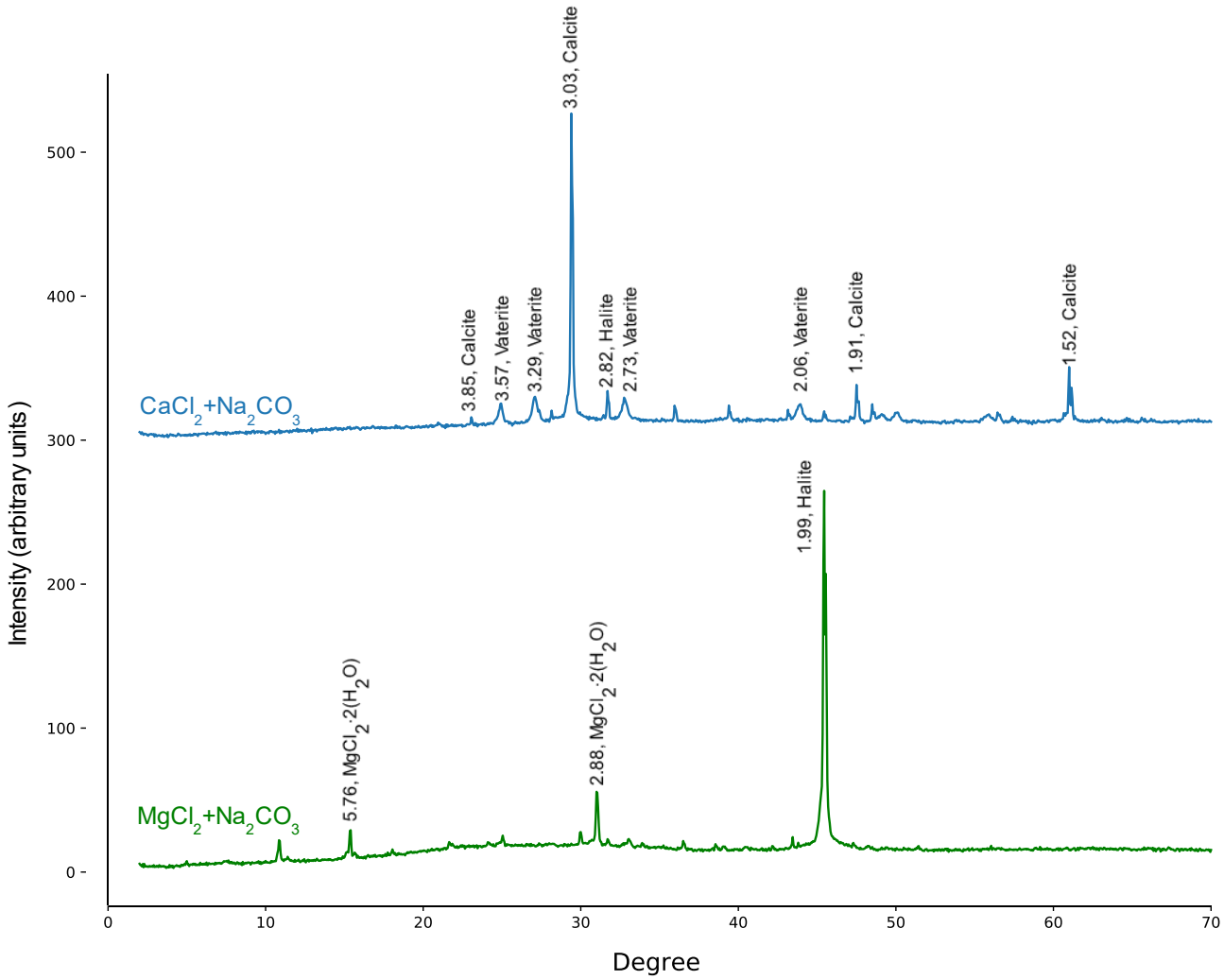

Figure 3-13 XRD patterns of precipitates formed after 2 mL carbonate/bicarbonate simulant reacting with 6 mL 0.1 M $CaCl_2$ and $MgCl_2$

3.2.1.2. Alkalinity neutralization of bauxite residue supernatant by Ca^{2+} and Mg^{2+}

The sodium concentration in the lake water roughly 0.1 M (Table 3-3). Therefore, 0.1 M NaCl concentration was used in the bauxite residue alkalinity neutralization treatment to mimic the ionic strength. MINTEQ simulation (Table 3-5) indicated that the water pH could be reduced by adding $CaCl_2$ or $MgCl_2$, and $CaCl_2$ showed a greater efficiency than $MgCl_2$ in reducing alkalinity. The simulation successfully predicted the pH of the liquid phase in the alkalinity neutralization of the Fe-oxide dominated bauxite residue, but deviated from the observed in Al-oxide dominated residue (Table 3-6). The XRD patterns (Figure 3-14) revealed that the mineral formation consumed the carbonate anion in the solution, causing the decrease of pH. Almost pure calcite precipitated when the $CaCl_2$ was added into the residue. Trace amounts of hydrotalcite ($Mg_6Al_2CO_3(OH)_{16}\cdot 4(H_2O)$) formed when $MgCl_2$ was added to the residue. The hydrotalcite precipitation in $MgCl_2$ treatment indicated the presence of aluminum ion in the pore water, but was not predicted from the MINTEQ simulation. The more intense hydrotalcite XRD peak in Fe-oxide dominated group strengthened our hypothesis aluminate might diffuse from the lower Fe-oxide dominated layer to the upper Al-oxide dominated layer due to the concentration gradient. Notable pH reduction was observed after adding $MgCl_2$ addition, some amorphous minerals might be also precipitated. But they could not be identified by X-ray diffraction.

Table 3-6 The pH of bauxite residue supernatant reacting with 6 mL 0.1 M NaCl, $CaCl_2$ and $MgCl_2$ after shaking 24 hours

Sample	Treatment		
	NaCl	$CaCl_2$	$MgCl_2$
Fe-oxide dominated	9.85 ± 0.01	7.47 ± 0.01	7.90 ± 0.01
Al-oxide dominated	8.76 ± 0.01	6.90 ± 0.01	7.65 ± 0.01

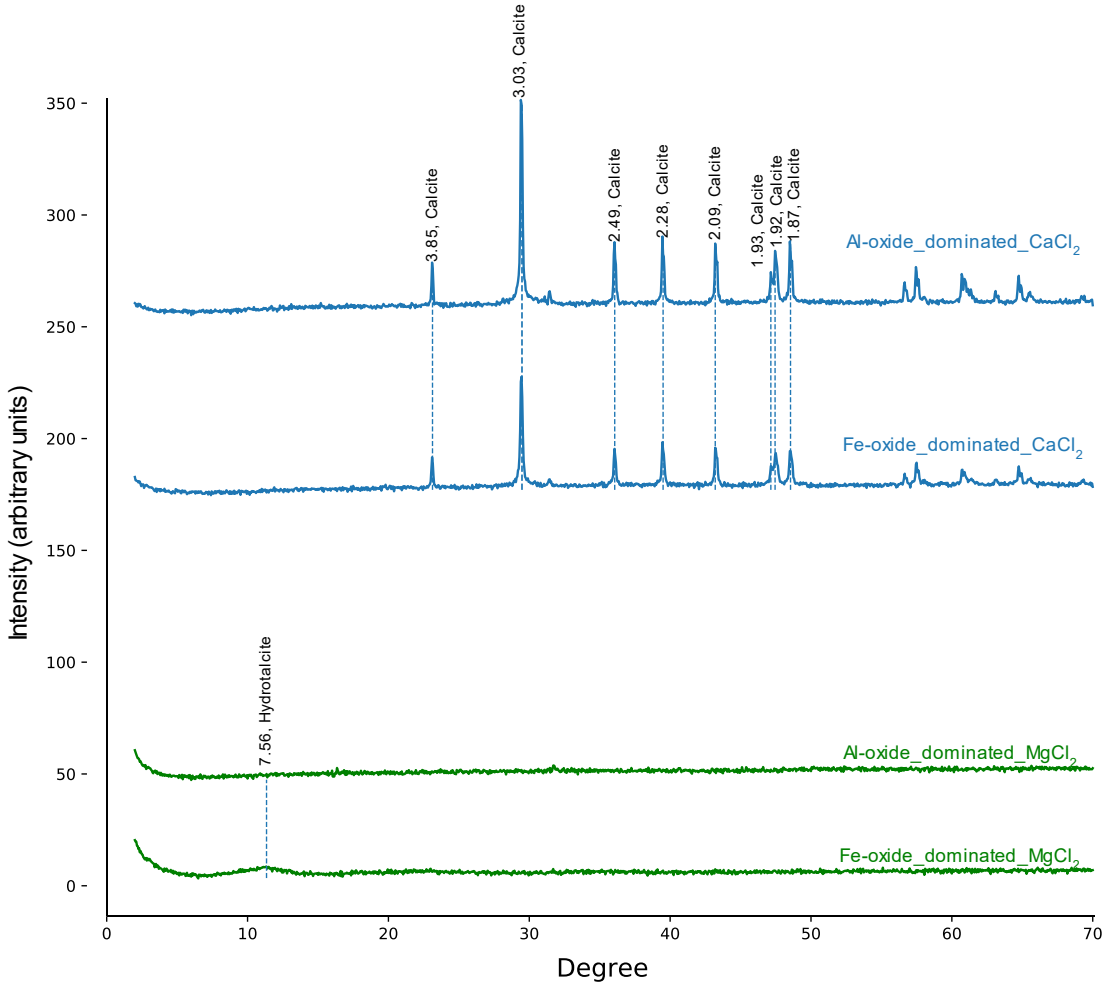

Figure 3-14 XRD spectra of Fe-oxide and Al-oxide dominated bauxite residue supernatants reacted with 6 mL 0.1 M $CaCl_2$ or $MgCl_2$ after three times washing by DI water

3.2.1.3. Alkalinity neutralization of bauxite residues by $CaCl_2$, $FeCl_3$, H_2SO_4, and NaH_2PO_4

Two approaches were used to neutralize the alkalinity of the bauxite residues: (1) Adding a divalent cation to form carbonate minerals to remove the carbonate and bicarbonate anions in the solution; (2) Adding acidic reagents to lower the pH and to convert carbonate to bicarbonate anion. For carbonate mineral formation method, only $CaCl_2$ was tested due to its higher efficiency comparing to the $MgCl_2$. For the acidic reagents: $FeCl_3$, H_2SO_4, and NaH_2PO_4 were selected to test their efficiency. A 0.1 M NaCl solution was chosen to be the background solution of control group based on sodium concentration from the lake water analysis result (Table 3-3).

The optimal pH after alkalinity neutralization should be between 7 and 8 because toxic metals (i.e. Fe, Mn, and other trace metal) are less soluble at this pH[54]. To determine optimal alkalinity neutralization concentration, three different concentrations of $CaCl_2$, $FeCl_3$, H_2SO_4, and NaH_2PO_4 were evaluated in neutralizing the alkalinity of the Fe-oxide dominated bauxite residue. Alkalinity neutralization of Fe-oxide dominated bauxite residue after the adding the above solutions was achieved (Table 3-7). It was observed that 0.01 M was the suitable concentration for $FeCl_3$, H_2SO_4, and 0.1 M for $CaCl_2$, and NaH_2PO_4.

The alkalinity neutralization results of Fe-oxide and Al-oxide dominated bauxite residue after the four solutions were summarized in Table 3-8. Comparable pH values in both groups after each treatment suggested that their solution chemistry was similar and might be close to the lake water.

3.2.1.3.1. Alkalinity neutralization by formation of carbonate minerals

Even though $CaCO_3$ formation was expected in $CaCl_2$ neutralization treatment, XRD and FTIR analysis of both Fe-oxide and Al-oxide dominated bauxite residues after $CaCl_2$ neutralization treatment (Figure 3-15, 3-16, 3-18 and 3-19) showed no difference from the control group (NaCl treatment). The predicted calcite precipitation did not yield visible changes on the XRD or FTIR patterns and might be attributed to the small quantity generated. Both the Fe-oxide and Al-oxide dominated bauxite residues already contained calcite before the alkalinity neutralization.

3.2.1.3.2. Alkalinity neutralization by adding acidic reagents or materials

No obvious mineral transformations were observed in either of the residues after $FeCl_3$, H_2SO_4, or NaH_2PO_4 treatments on XRD or FTIR patterns (Figure 3-15, 3-16, 3-18 and 3-19). Similar distributions of particle size in $CaCl_2$, NaCl, H_2SO_4 treatment were observed (Figure 3-17). The particle size distribution for most of the Fe-oxide dominated bauxite residue after all treatments was less than 2 μm. It was noteworthy that the high clay proportion in this long-term storage bauxite residue compared to the reported size of residue sand (100-1000 μm) and fine-textured mud (1-10 μm) in an early study[55]. Smaller particles in DI water treatment might be attributed to the dissolution of salt connecting between particles. Large particle size (20 and 36 μm) in Al-oxide dominated bauxite residue could be explained by the aggregate formation during Al-oxide mineral crystallization (Figure 3-20).

Table 3-7 The pH of Fe-oxide dominated bauxite residue after different concentration of alkalinity neutralization

Treatment	Concentration (M)			
	0.001	0.01	0.1	1
$CaCl_2$		9.2 ± 0.04	7.3 ± 0.01	6.6 ± 0.02
NaH_2PO_4		9.5 ± 0.04	7.5 ± 0.01	6.3 ± 0.02
$FeCl_3$	9.8 ± 0.01	8.0 ± 0.03	6.0 ± 0.01	
H_2SO_4	9.8 ± 0.00	7.6 ± 0.02	6.4 ± 0.03	

Table 3-8 The pH of optimal alkalinity neutralization stock solutions, Fe-oxide and Al-oxide dominated bauxite residue after neutralization treatments

Sample		Treatment					
		DI	NaCl (Control)	$CaCl_2$	H_2SO_4	$FeCl_3$	NaH_2PO_4
Stock solution	Concentration (M)	N/A	0.1	0.1	0.01	0.01	0.1
	pH	6.0	6.2	5.8	1.9	2.3	4.5
Fe-oxide dominated	pH	9.9 ± 0.03	9.5 ± 0.03	7.3 ± 0.04	7.3 ± 0.03	7.6 ± 0.10	7.4 ± 0.01
Al-oxide dominated	pH	9.5 ± 0.04	9.26 ± 0.02	7.0 ± 0.10	7.5 ± 0.02	7.8 ± 0.04	7.4 ± 0.01

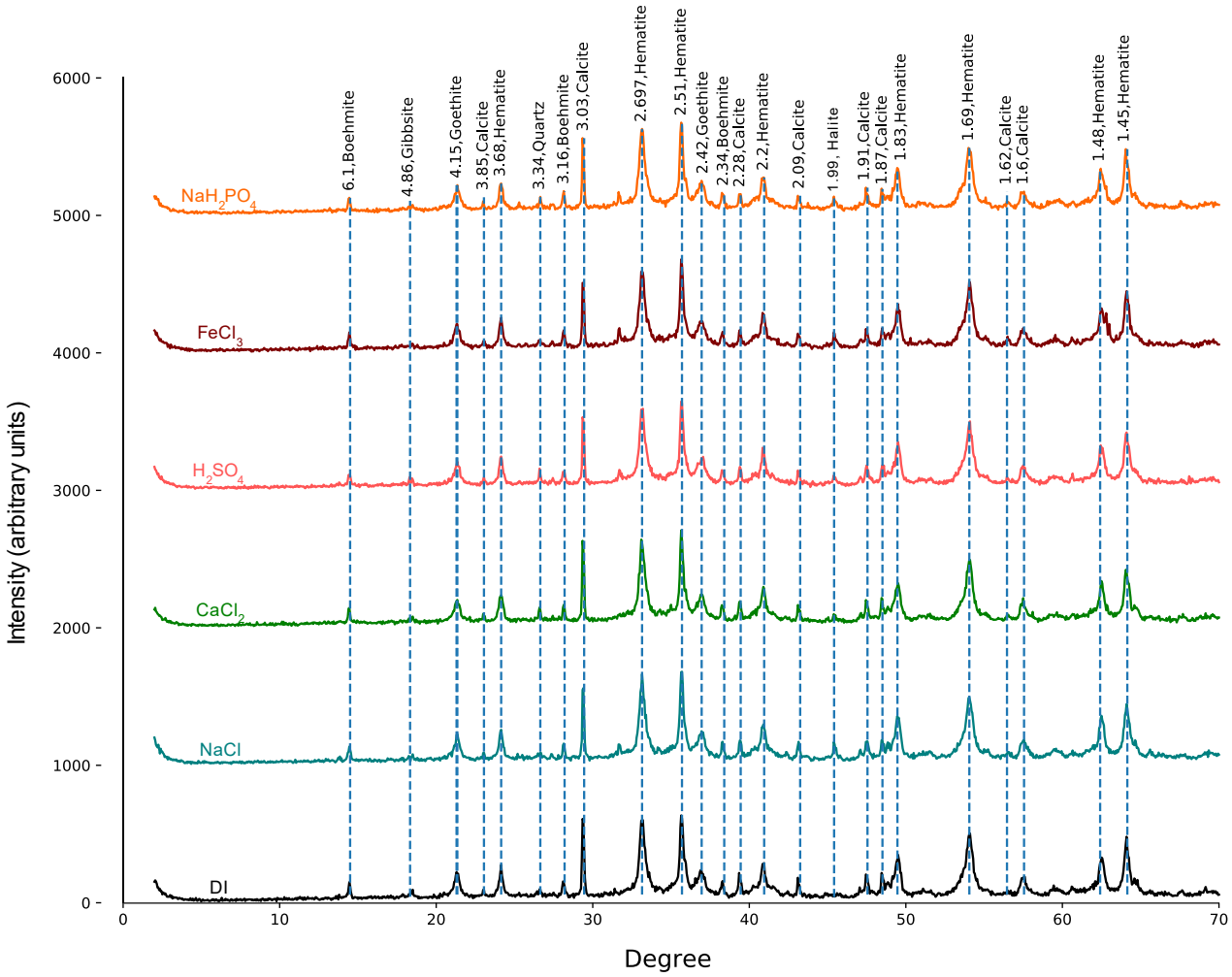

Figure 3-15 XRD spectra of alkalinity neutralized Fe-oxide dominated bauxite residue

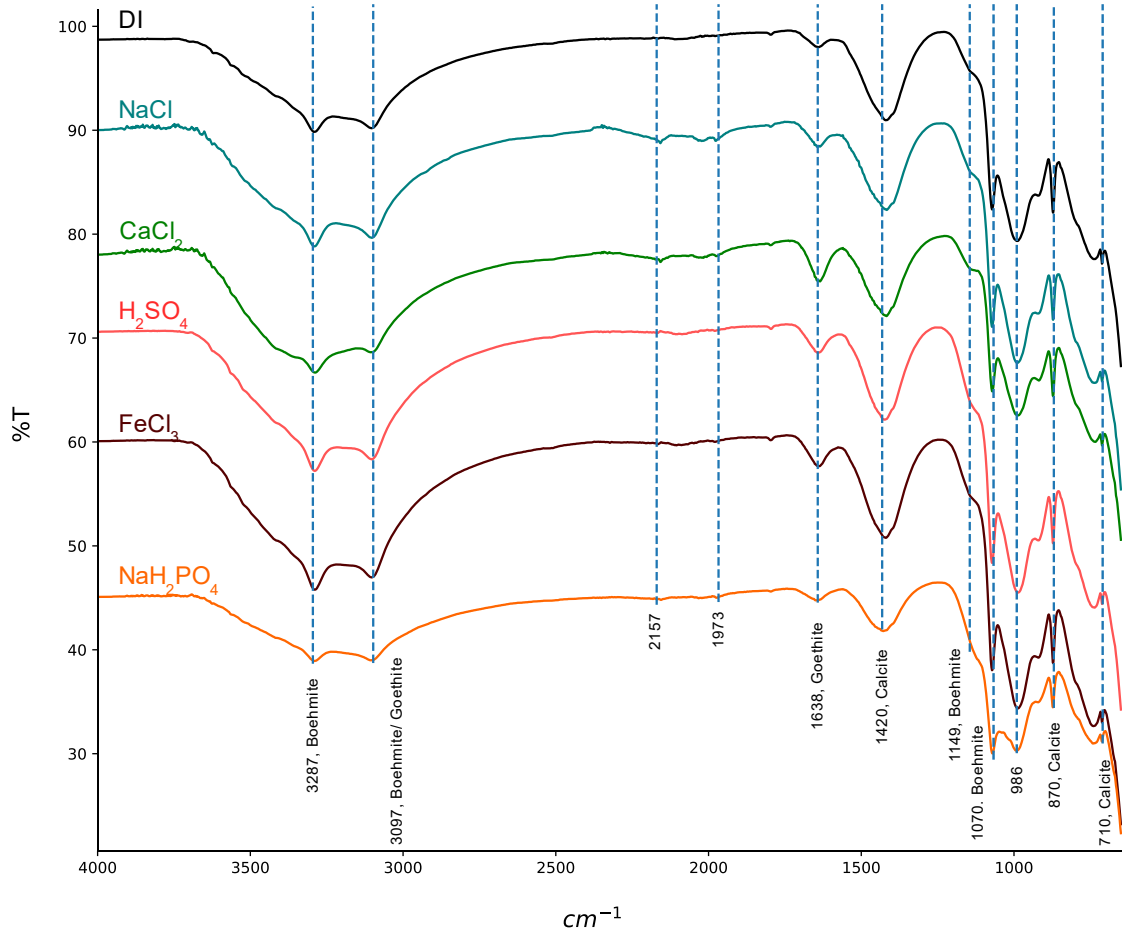

Figure 3-16 FTIR of alkalinity neutralized Fe-oxide dominated bauxite residue

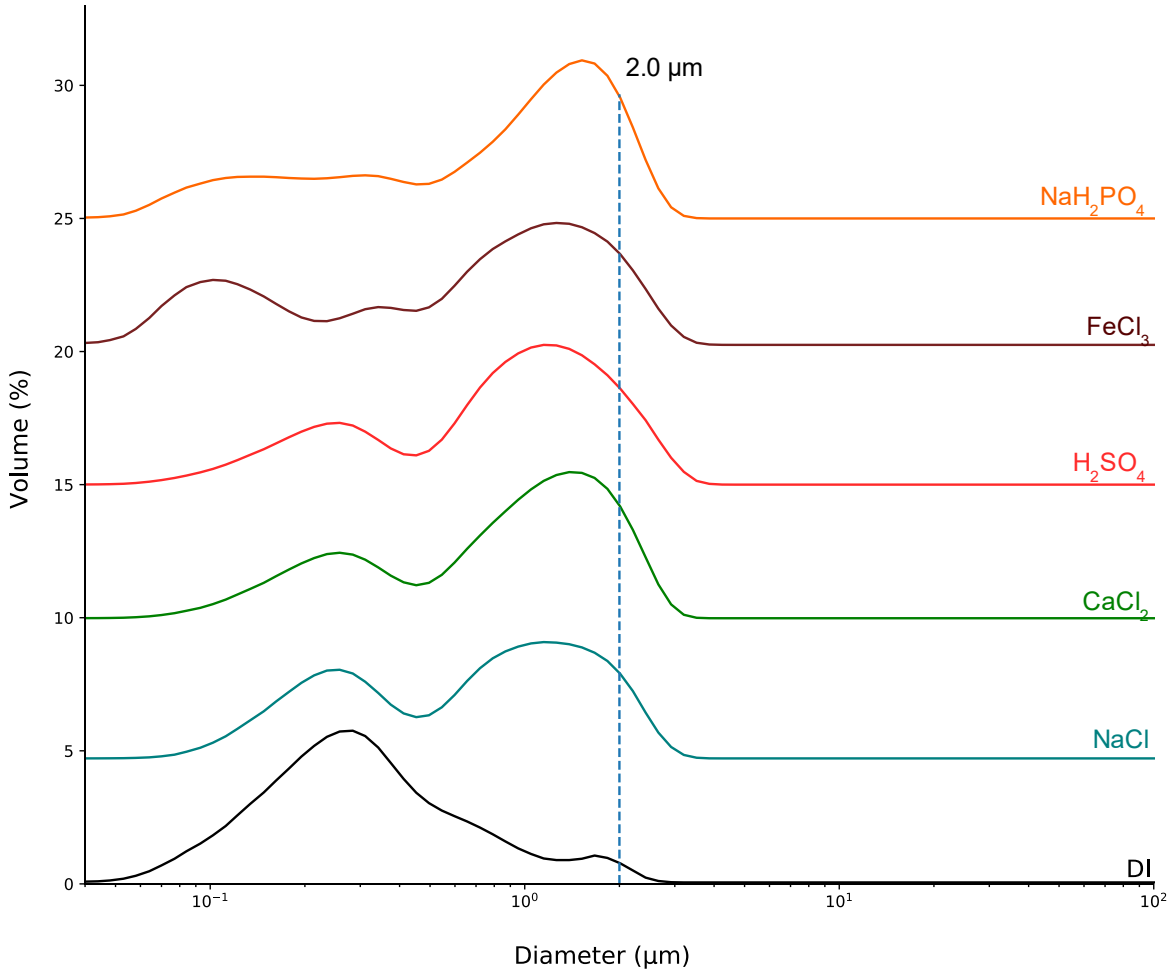

Figure 3-17 Particle size analysis of alkalinity neutralized Fe-oxide dominated bauxite residue

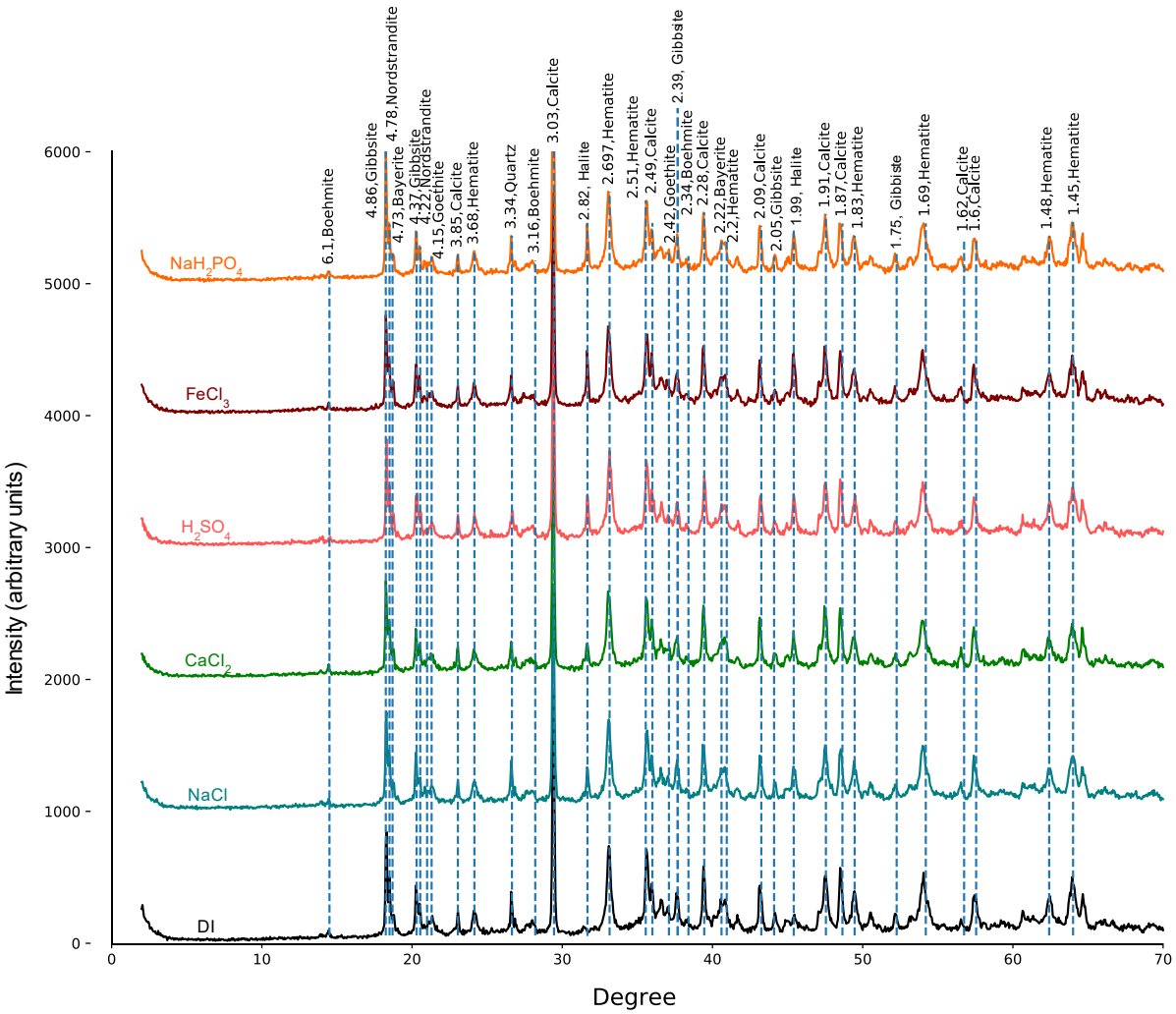

Figure 3-18 XRD spectra of alkalinity neutralized Al-oxide dominated bauxite residue

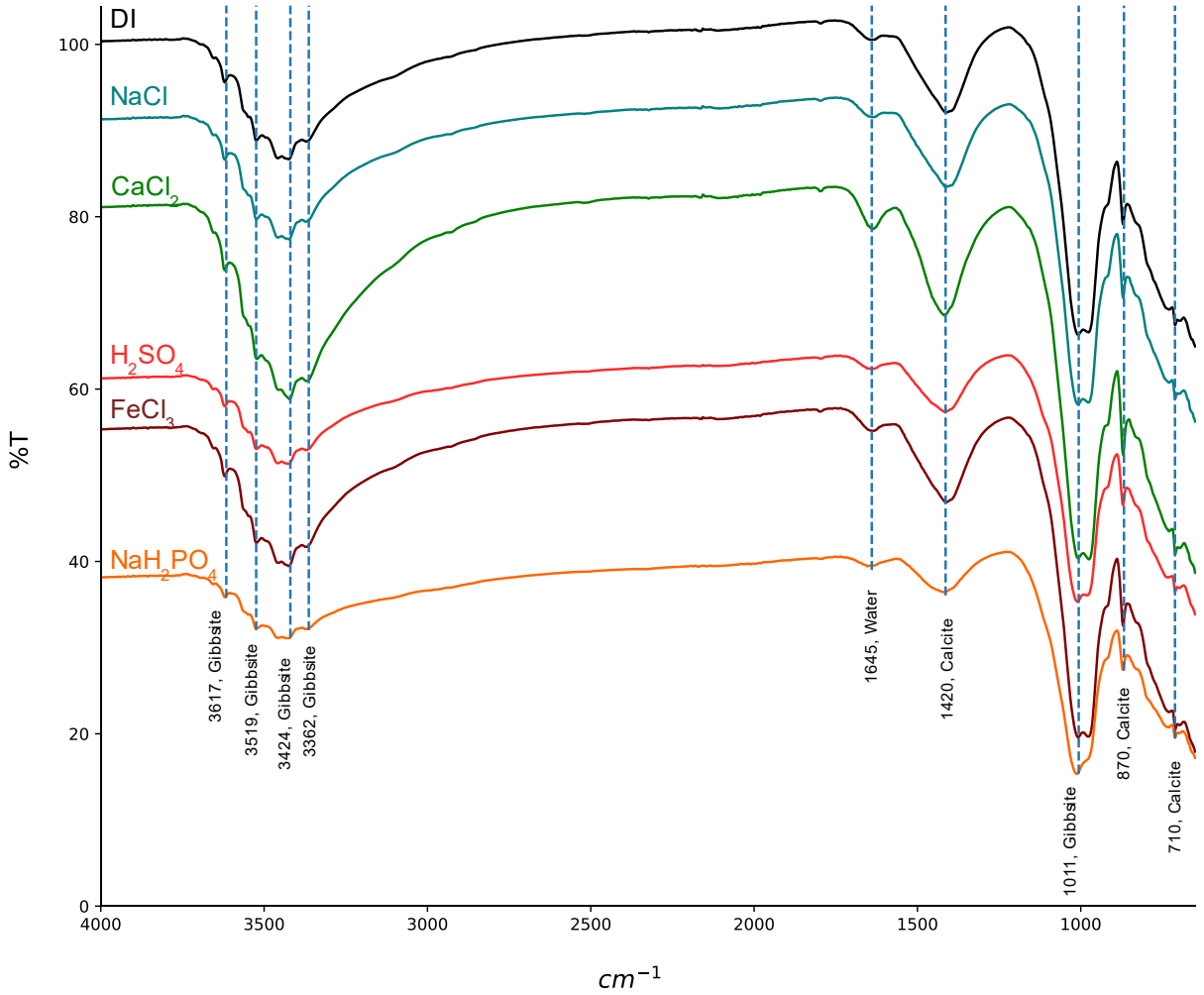

Figure 3-19 FTIR of alkalinity neutralized Al-oxide dominated bauxite residue

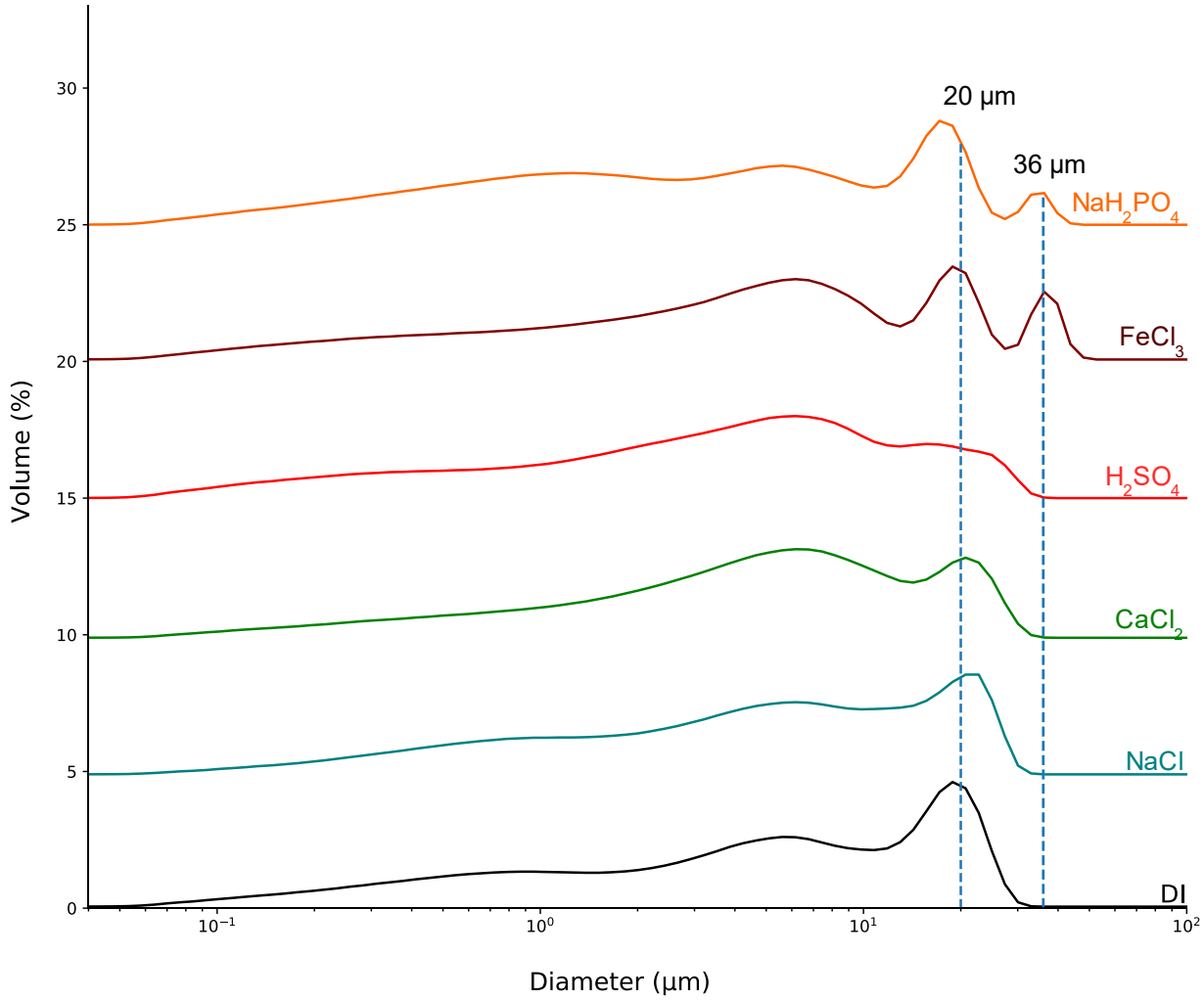

Figure 3-20 Particle size analysis of alkalinity neutralized Al-oxide dominated bauxite residue

3.2.2. Settling performance of Fe-oxide dominated bauxite residue after alkalinity neutralization

Particle settling evaluation was conducted on the Fe-oxide dominated residue only due to its similarity to the typical bauxite residue. In addition to the function of neutralizing alkalinity, polyvalent cations like Ca^{2+} and Fe^{3+} should be able to screen the negative charges on iron and aluminum oxide particles, reduce the double layer thickness, and promote the aggregation. Phosphate might be able to connect iron or aluminum oxide particles by adhering to two surfaces. It was reported that H_2SO_4 could enhance the macro-aggregate formation in addition to alkalinity neutralization[21]. The NaCl treatment served as the control to simulate the high ionic strength of the lake water. Effect of surfactant and polyacrylamide of different charge types as evaluated before and after alkalinity neutralization treatments were examined. Settling performance was quantified by settling ratio, which was calculated from percentage of the supernatant volume divided by the original volume.

3.2.2.1. Bauxite residue settling after adding sulfuric acid, polyvalent cations, or phosphate

Ionic strength of the background solution was important in the setting of the residues (Figure 3-21). Settling ratios for $FeCl_3$, H_2SO_4 prepared in distilled water were significantly lower than those in 0.1 M NaCl, suggesting dispersion of the particles in the diluted solution. Thus, $FeCl_3$, H_2SO_4 and NaH_2PO_4 were prepared in 0.1 M NaCl to maintain the high ionic strength. This could also reflect the high ionic strength of the

lake water in practical application scenario—adding the solid form of chemicals into the lake water directly.

Although macro-aggregate formation after reacting with H_2SO_4 was reported, and polyvalent cations, such as calcium or iron, might help the agglomeration of bauxite residue particles and accelerate particle settling[56]. No significant settling improvement was observed after applying Fe^{3+} or Ca^{2+}. The control treatment (NaCl) was even better regarding the final settling ratio (Figure 3-22). The settling ratios after different neutralization treatments ($CaCl_2$, $FeCl_3$, H_2SO_4 and NaH_2PO_4) were similar, which indicated that pH was likely to be major factor controlling the settling. However, when comparing to the DI water, all treatments successfully accelerated the particle settling, most likely by reducing the diffuse double layer due to their high ionic strength and the residue electrostatic repulsion of the Fe- or Al- oxide particles due to the reduced pH.

It was unexpected that alkalinity neutralization treatments did not promote the settling of the residue particles compared to the NaCl control treatment. One possible explanation was the flocs size of the bauxite residue. Although similar particle sizes after the four alkalinity neutralization treatments were observed in Figure 3-17, the dispersion caused by DI water in the particle size analysis might alter the macro-structure. To avoid the inference from DI water, treated bauxite residues diluted in the background solution (0.1 M NaCl or $CaCl_2$) were placed on the glass slides and gently shook by hand after 5 minutes settling (Figure 3-23). Two distinct differences were observed: (1) distilled water dispersed bauxite residue particles dramatically; (2) alkalinity neutralization treatments would cause the particles to be loosely distributed. Deteriorating settling

performance of DI water might be explained by the dissolution of salts between particles, which also was detected in the particle size analysis (Figure 3-17). SEM image (Figure 3-7) revealed that bauxite residue was composed of fine particles (0.1~0.5 μm) in macro-aggregate (~5 μm). Loose-packed particles after neutralization treatments might indicate the decomposition of macro-aggregate. Smaller particles appeared in the H_2SO_4-treated bauxite residue comparing to the control group (NaCl) under optical microscope proved the break-down of the macroaggregate (Figure 3-24).

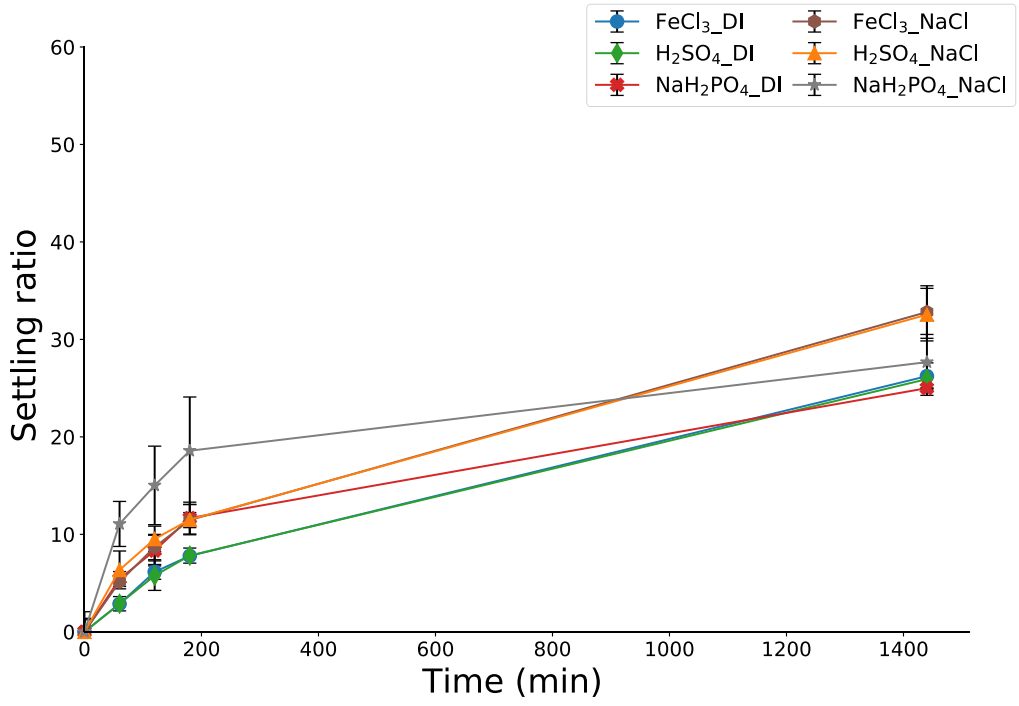

Figure 3-21 Settling performance of Fe-oxide dominated bauxite residue after adding $FeCl_3$, H_2SO_4 and NaH_2PO_4 prepared in DI or 0.1 M NaCl. Higher settling ratio suggested faster settling.

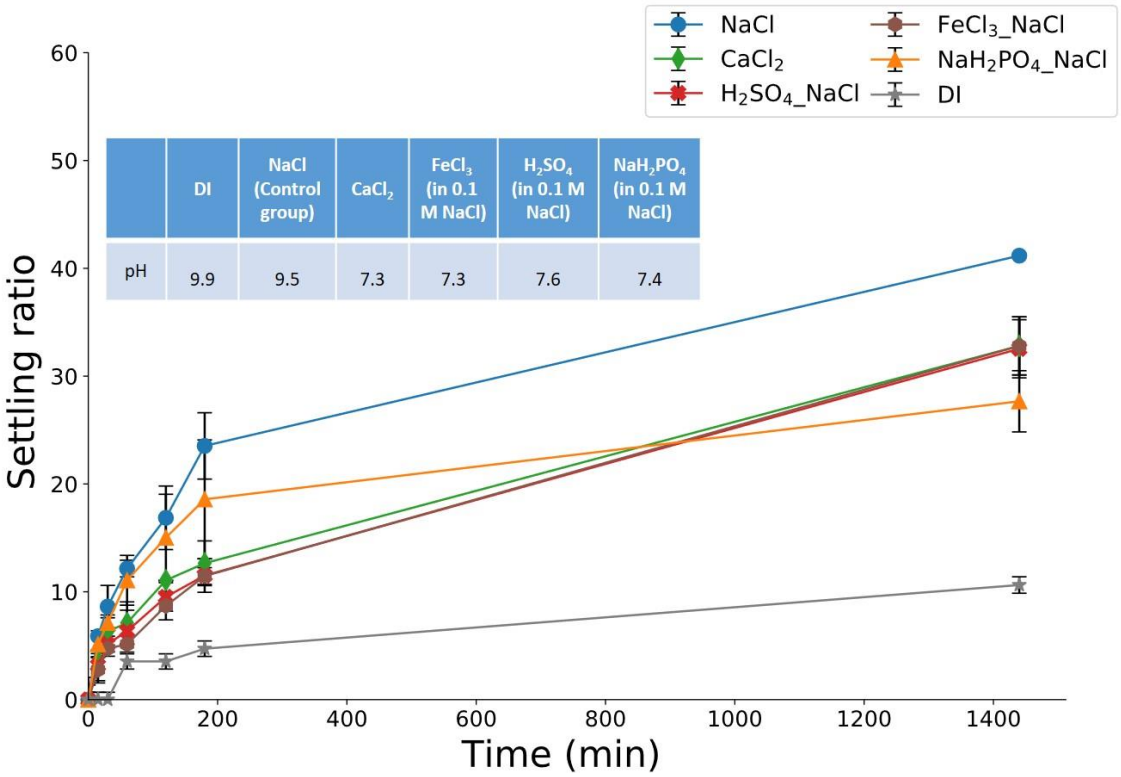

	DI	NaCl (Control group)	$CaCl_2$	$FeCl_3$ (in 0.1 M NaCl)	H_2SO_4 (in 0.1 M NaCl)	NaH_2PO_4 (in 0.1 M NaCl)
pH	9.9	9.5	7.3	7.3	7.6	7.4

Figure 3-22 Settling performance of neutralized Fe-oxide dominated bauxite residue

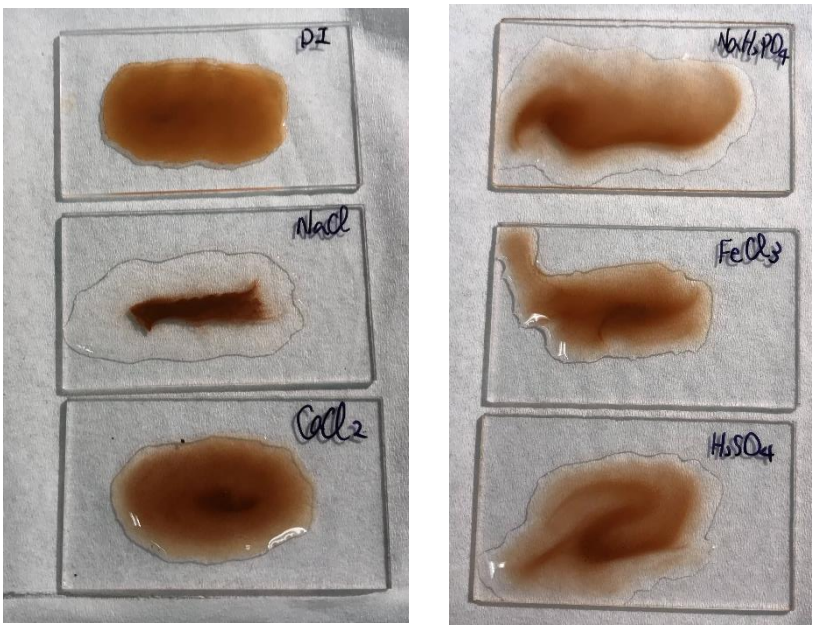

Figure 3-23 Neutralized Fe-oxide dominated bauxite residue diluted in the background solution on the glass slides after shaking by hand

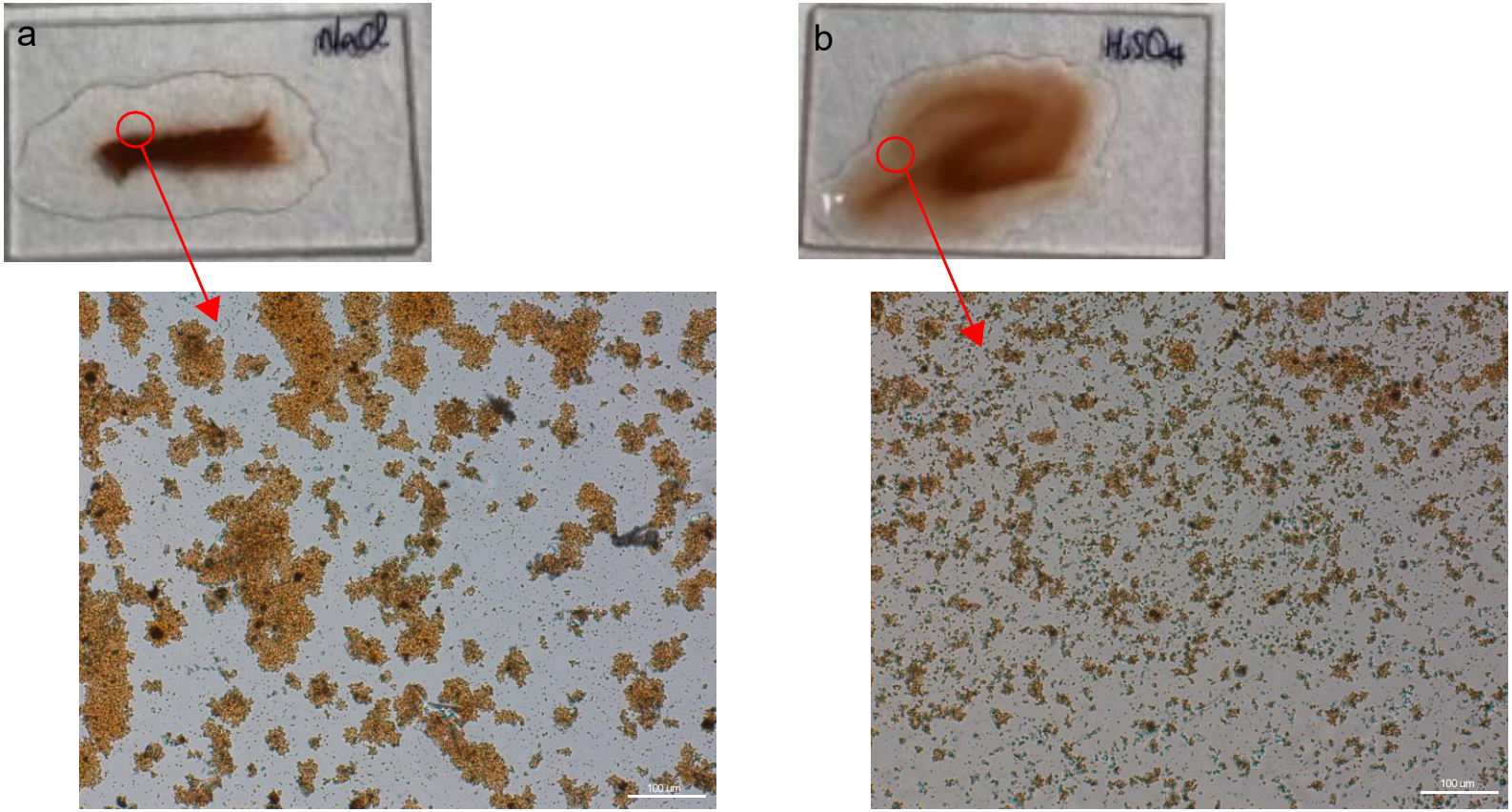

Figure 3-24 Optical images of (a) NaCl (control group); (b) H_2SO_4 neutralized Fe-oxide dominated bauxite residue

3.2.2.2. Improving neutralized Fe-oxide dominated bauxite residue settling by adding polymers

3.2.2.2.1. Effect of polymer charge and concentration on the settling of the residue

Both neutral and anionic PAM efficiently flocculate bauxite residue when the polymer concentration was greater than 250 ppm (mg PAM/ kg bauxite residue) for the anionic and 500 ppm for the neutral PAM, while cationic PAM only showed settling improvement at 500 ppm dosage.

More extended structure by electrostatic repulsion force at alkaline pH may result in the better settling performance of anionic PAM in comparison with cationic and neutral PAM. Higher affinity of neutral PAM suppressed the extension of polymer, less bridging between particles, thus deteriorated the settling performance[57]. This might also explain the poor performance of cationic PAM. The similar final settling ratio between the control group (Figure 3-22) and PAM treatment (Figure 3-25) indicated the treatments did not enhance the consolidation after 24 hours settling. ” Gel-like” Fe-oxide dominated bauxite residue flocs formed after mixing with PAM after NaCl treatment (Figure 3-26 (b)).

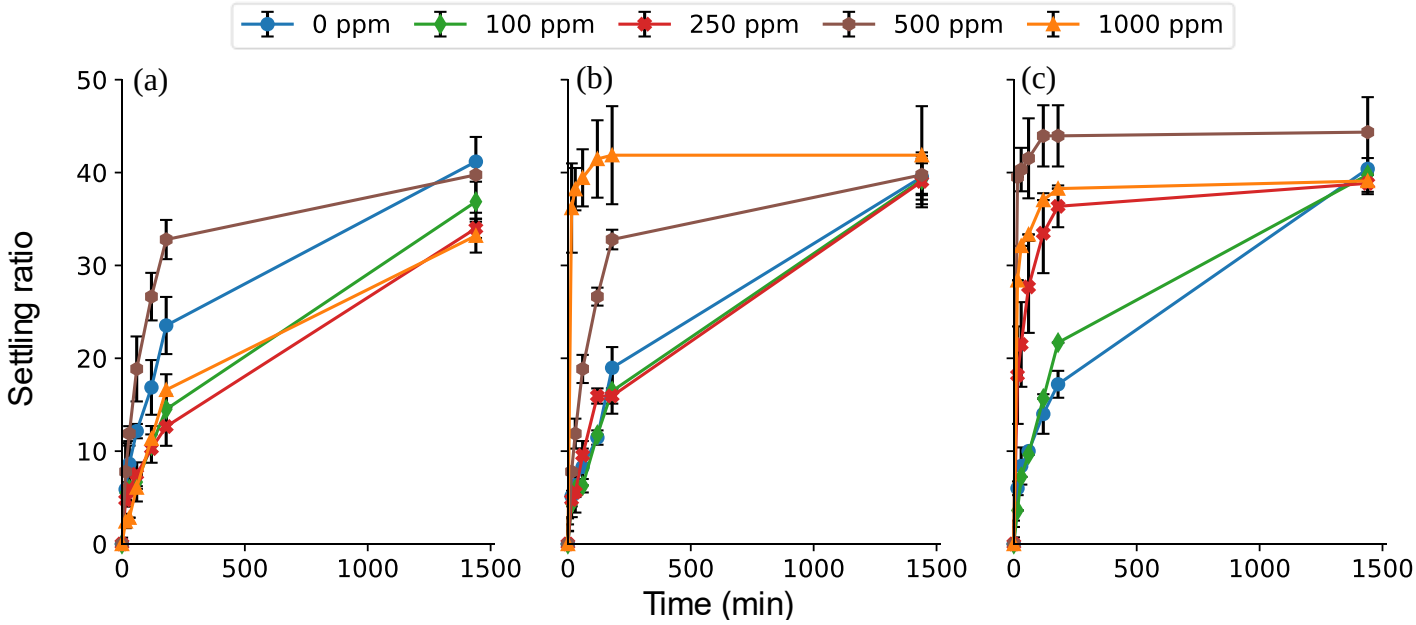

Figure 3-25 Settling ratio of 0.1 M NaCl Fe-oxide dominated bauxite residue after adding different concentration (0, 100, 250, 500, 1000 ppm (mg PAM/kg bauxite residue)) of (a) cationic, (b) neutral, and (c) anionic PAM

Figure 3-26 Fe-oxide dominated bauxite residue mixing with (a) 25 ppm SDS in 0.1 M NaCl; 1000 ppm neutral PAM after (b) NaCl, (c) $CaCl_2$, (d) H_2SO_4, (e) $FeCl_3$, (f) NaH_2PO_4 treatments

3.2.2.2.2. Effect of alkalinity neutralization on polyacrylamide flocculation of bauxite residue

Three dosages (0, 250, 1000 ppm = mg PAM/kg bauxite residue slurry) of polymers were selected according to the flocs difference from control group experiment (NaCl): no large flocs formed under 250 ppm, but the settling rate increased; visible flocs generated and improved the settling performance when applying 1000 ppm polymers.

Cationic PAM only demonstrated improvement on the settling ratio in 250 ppm after $CaCl_2$ treatment (Figure 3-27). Carbonate ions consumed by calcium could assist the extension of polymer chain, thus potentially enhance the cationic PAM settling performance. Both neutral and anionic PAM significantly improved settling of the $CaCl_2$-, $FeCl_3$-, H_2SO_4- neutralized bauxite residue (Figure 3-28 and 3-29). The only inconsistent result was NaH_2PO_4 treatment, except for 250 ppm neutral PAM, neither neutral nor anionic PAM enhanced the settling. Reduced settling performance might be associated the surface property changes induced by the adsorption of phosphate on iron or aluminum oxide surface, which hindered the approach of the polymer chains. Large, stable, and loose flocs (Figure 3-26 (c)~(e)) formed after adding 1000 ppm neutral or anionic PAM in $CaCl_2$, $FeCl_3$, H_2SO_4 neutralized Fe-oxide dominated bauxite residues, which caused the settling ratios to be constant during the monitored period. In addition, some liquid would be entrapped by those flocs, misleading the calculation of settling ratios. Thus, settling volumes instead of settling ratios were further analyzed by two-way ANOVA to demonstrate the effect of pH and electrolyte.

The 1 hour and 24 hours settling volumes of various treatments after adding 1000 ppm different PAM were shown in Figure 3-30. In almost all treatments, neutral and anionic PAM could promote the settling, except NaH_2PO_4 due to the possible surface change mentioned above. In current study, the expected synergistic effect between PAM and polyvalent cations (Ca^{2+}, Fe^{3+}) from wastewater treatment industry was not observed[23]. No significant difference in 1 hour settling volumes was observed among $CaCl_2$, $FeCl_3$, H_2SO_4 treatments, suggesting that the pH might be the major factor affecting the PAM efficiency. After 24 hours, final consolidation volumes of alkalinity neutralized bauxite residues increased after adding the PAM (Figure 3-30).

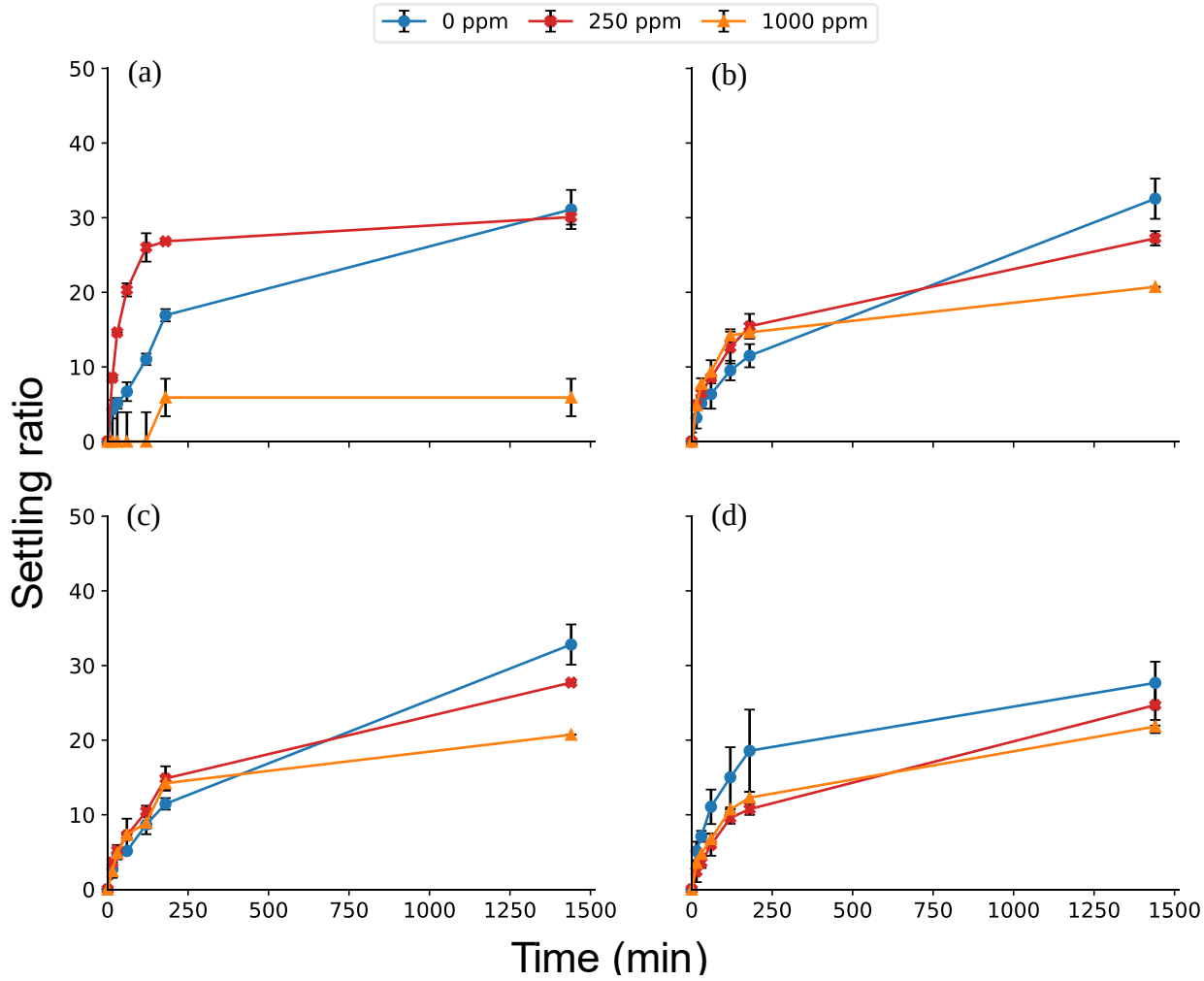

Figure 3-27 Settling ratio of (a) 0.1 M $CaCl_2$, (b) 0.01 M H_2SO_4, (c) 0.01 M $FeCl_3$, (d) 0.1 M NaH_2PO_4 neutralized Fe-oxide dominated bauxite residue after adding 0, 250, 1000 ppm (mg PAM/ kg bauxite residue) cationic PAM

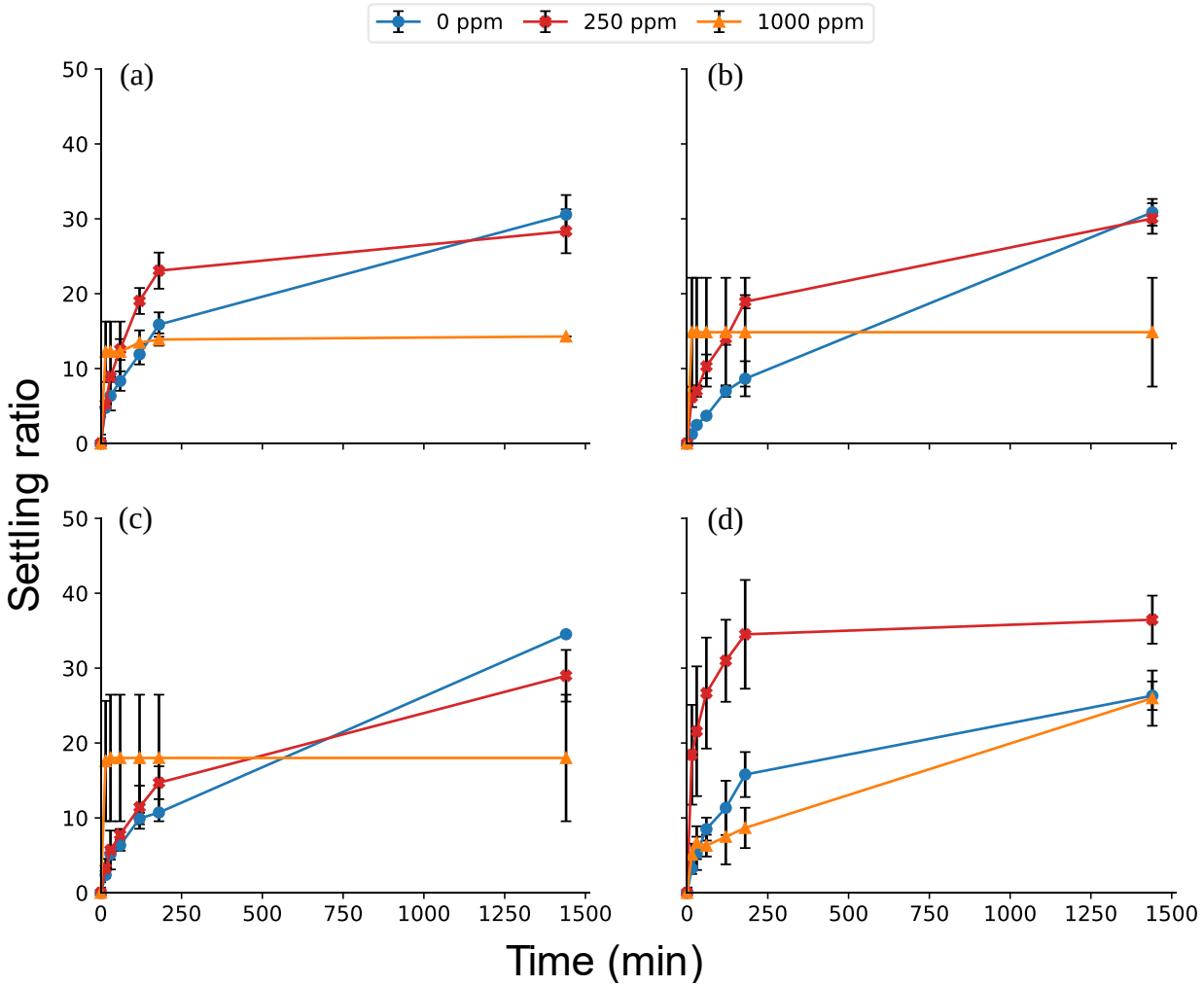

Figure 3-28 Settling ratio of (a) 0.1 M $CaCl_2$, (b) 0.01 M H_2SO_4, (c) 0.01 M $FeCl_3$, (d) 0.1 M NaH_2PO_4 neutralized Fe-oxide dominated bauxite residue after adding 0, 250, 1000 ppm (mg PAM/ kg bauxite residue) neutral PAM

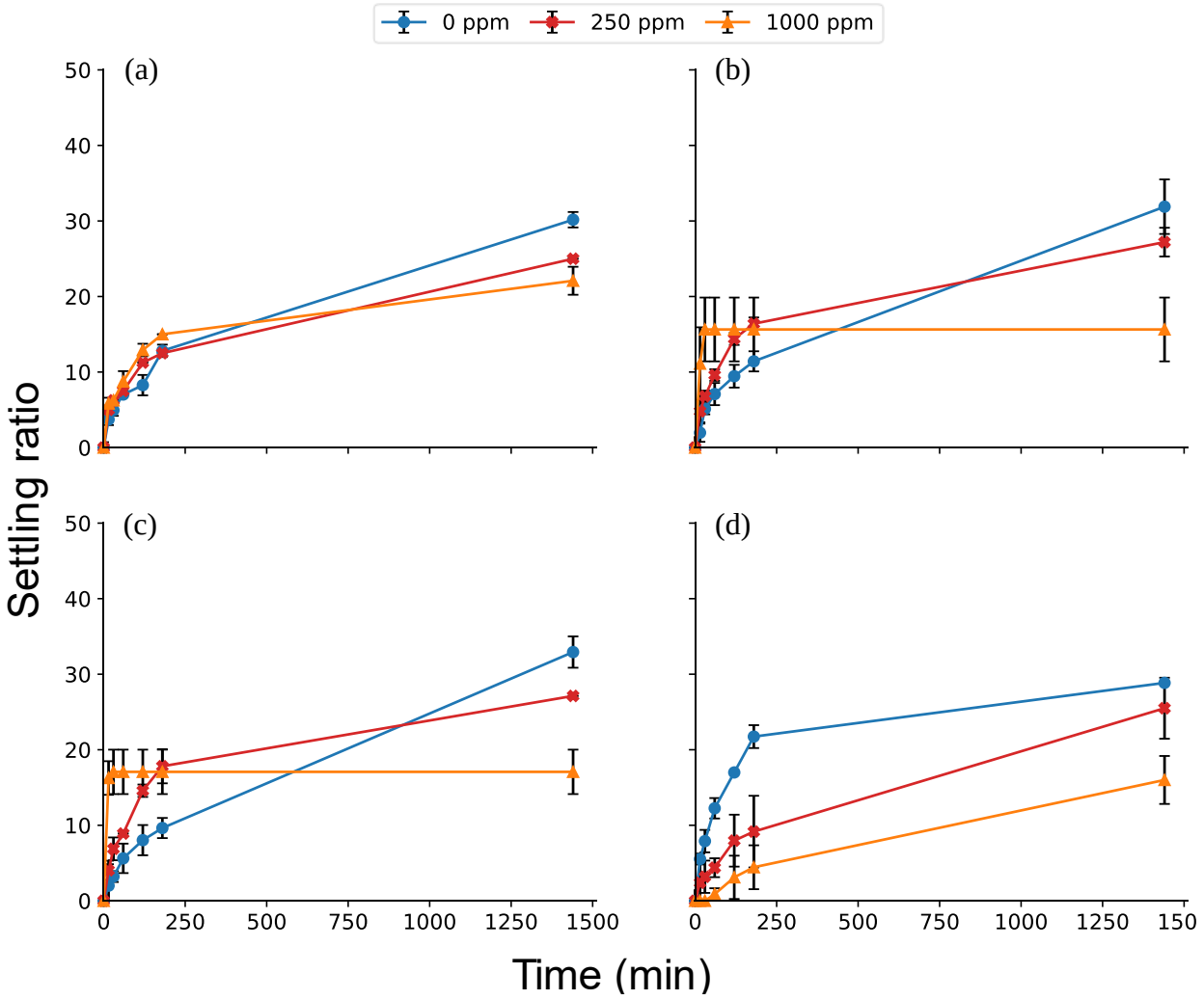

Figure 3-29 Settling ratio of (a) 0.1 M $CaCl_2$, (b) 0.01 M H_2SO_4, (c) 0.01 M $FeCl_3$, (d) 0.1 M NaH_2PO_4 neutralized Fe-oxide dominated bauxite residue after adding 0, 250, 1000 ppm (mg PAM/ kg bauxite residue) neutral PAM

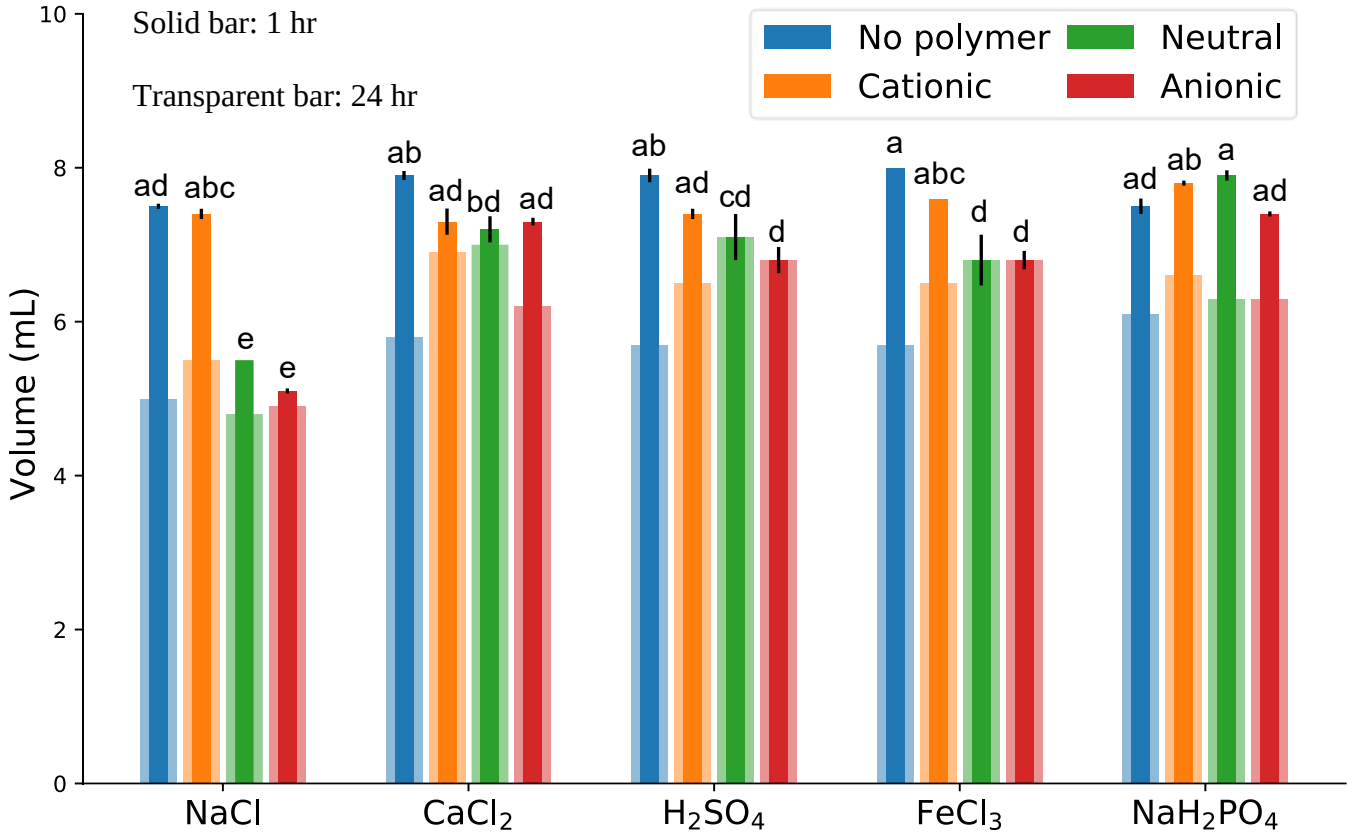

Figure 3-30 The 1 hour and 24 hours settling volumes of various neutralized Fe-oxide dominated bauxite residue after adding 1000 ppm different charge type PAM

Note. Values are means ± SEM, n = 3 per treatment group. [a-e]1hr volumes without a common superscript letter differ ($P < 0.05$) as analyzed by two-way ANOVA and the LSD test with Bonferroni correction.

3.2.2.3. Improving neutralized Fe-oxide dominated bauxite residue settling by adding surfactants

3.2.2.3.1. Surfactant charge effect

Two surfactants, an anionic surfactant (SDS) and a cationic surfactant (BDTDA), were evaluated in bauxite residue settling improvement test. Decreasing viscosity by adding surfactant into bauxite residue was verified, and the anionic surfactant prepared in sodium hydroxide was the best method to reduce viscosity because the cation sodium served as the bridge between particles and anionic surfactants[31]. According to the Stokes' Law, reducing viscosity could promote the settling, thus addition of surfactants was expected to enhance settling.

To simulate the application condition and maintain high ionic strength, both surfactants were prepared in the 0.1 M NaCl. It was found that SDS was able to accelerate the settling even at a concentration as low as 5 ppm (Figure 3-31 (a)), while BDTDA did not have any significant effect in the concentration range tested (Figure 3-31 (b)). The poor ability of BDTDA to improve settling performance might be attributed to the incomplete dissolution of the surfactant in 0.1 M NaCl compared to DI water (Figure 3-33 (a)). Although 50 ppm SDS appeared to be the optimal concentration from its highest settling ratio, a cloudy suspension was observed (Figure 3-33 (b)), which might be due to the formation of micelles and bubbles created by excessive SDS. Therefore, only up to 25 ppm of SDS was conducted for the settling improving experiments.

Surfactant SDS flocs were noticed after storing for a few days (Figure 3-32 (a)). This visible aggregate might result from accumulation of several micelles. The critical micelle concentration (CMC) of SDS was estimated to be 8.5 mM at 29°C and the CMC remained constant with the range 5-10[58, 59]. The stock solution in this study had a concentration of 17 mM and pH at 7-10; therefore, micelles should form in all the SDS experiments. SDS dissolved in 0.1 M $CaCl_2$ was examined to mimic the preparation in seawater environment. High calcium concentration induced precipitation of the surfactant when 0.05 g SDS was dissolved in the 0.1 M $CaCl_2$ (Figure 3-32 (b)), similar phenomenon was reported before[60]. To eliminate the influence of calcium ions, SDS prepared in 0.1 M NaCl was used for settling improving experiments.

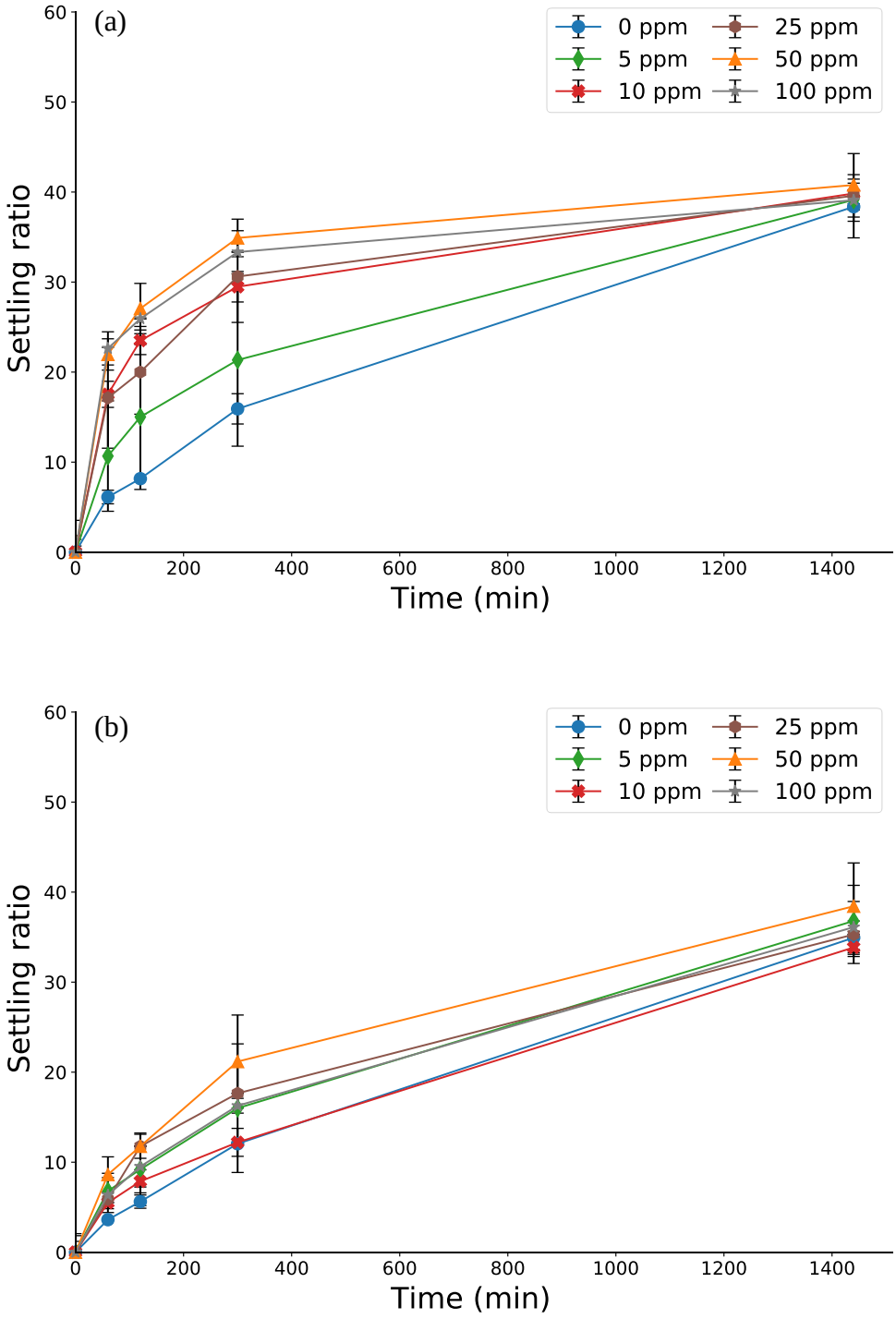

Figure 3-31 Settling ratio of Fe-oxide dominated bauxite residue after adding 0, 5, 10, 25, 50, 100 ppm (mg surfactant/ kg bauxite residue) (a) SDS, and (b) BDTDA

a) b)

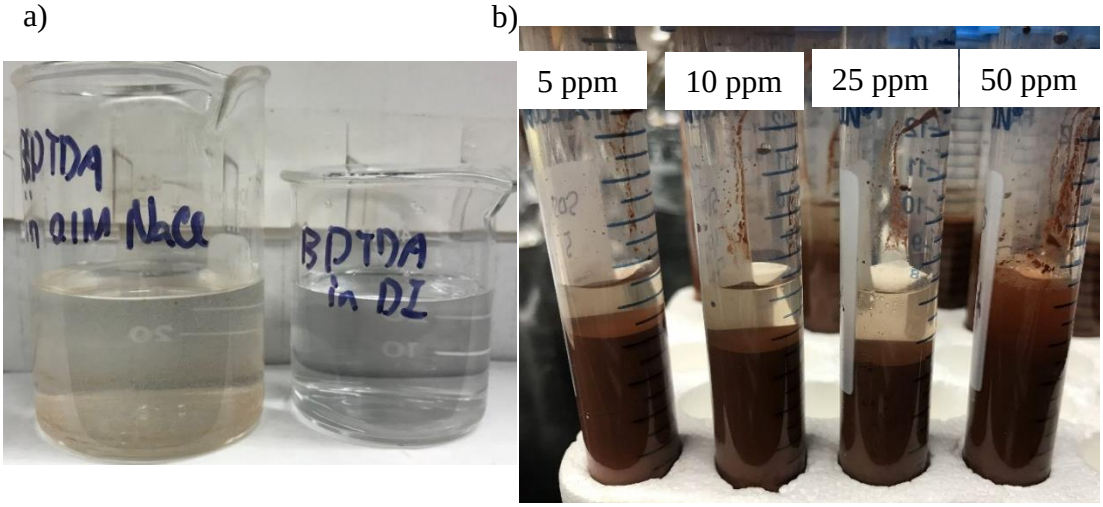

Figure 3-32 (a) BDTDA dissolved in 0.1 M NaCl or DI water, (b) Fe-oxide dominated bauxite residue settled 24 hr after adding 5, 10, 25, 50 ppm SDS

a) b)

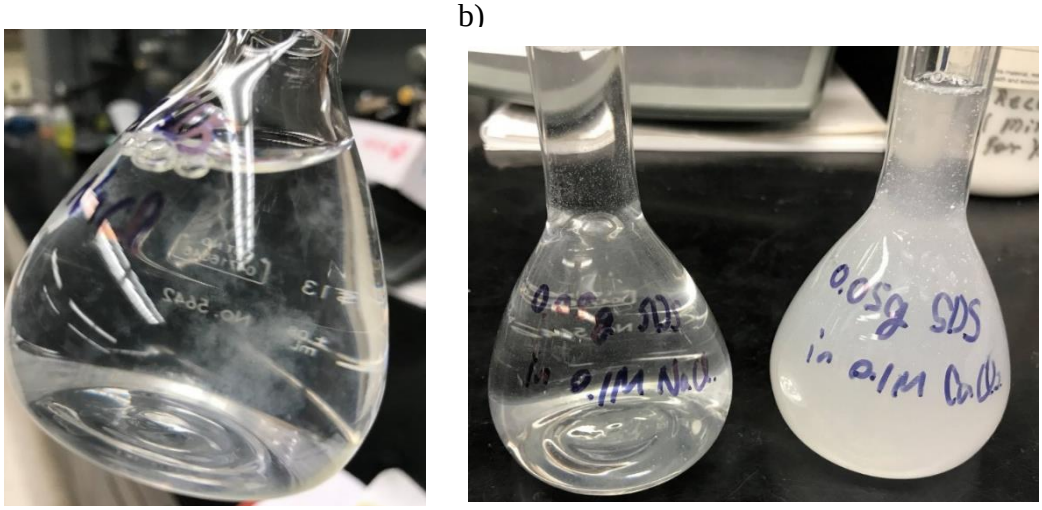

Figure 3-33 (a) Observed SDS cluster in 0.1 M NaCl after few days' storage; (b) SDS dissolved in 0.1 M NaCl or 0.1 M $CaCl_2$

3.2.2.3.2. Reduced efficiency of surfactant SDS in improving particle settling after alkalinity neutralization

After alkalinity neutralization, surfactant SDS lost the ability to accelerate the settling after either $CaCl_2$ or H_2SO_4 treatment (Figure 3-34). A similar lack of improvement in settling on seawater neutralized bauxite residue by the anionic surfactant was observed before, and it was attributed to the alteration of surface properties[31]. The detrimental effect of calcium ions on SDS settling performance could also be associated with the formation of calcium-surfactant precipitates mentioned before. The H_2SO_4 treatment was used to investigate the pH effect of SDS settling performance and the poor performance at neutral pH might be ascribed to the decrease negative charge on the surface. Although the smaller particles from aggregate decomposition discussed above might reduce efficiency of the SDS, the settling performance should improve if the SDS interacted with the surface of particles. Thus, unsuccessful results from both $CaCl_2$ and H_2SO_4 alkalinity neutralization treatments indicated the pH might alter the surface of particles and would be the major factor affecting the settling improving of surfactants.

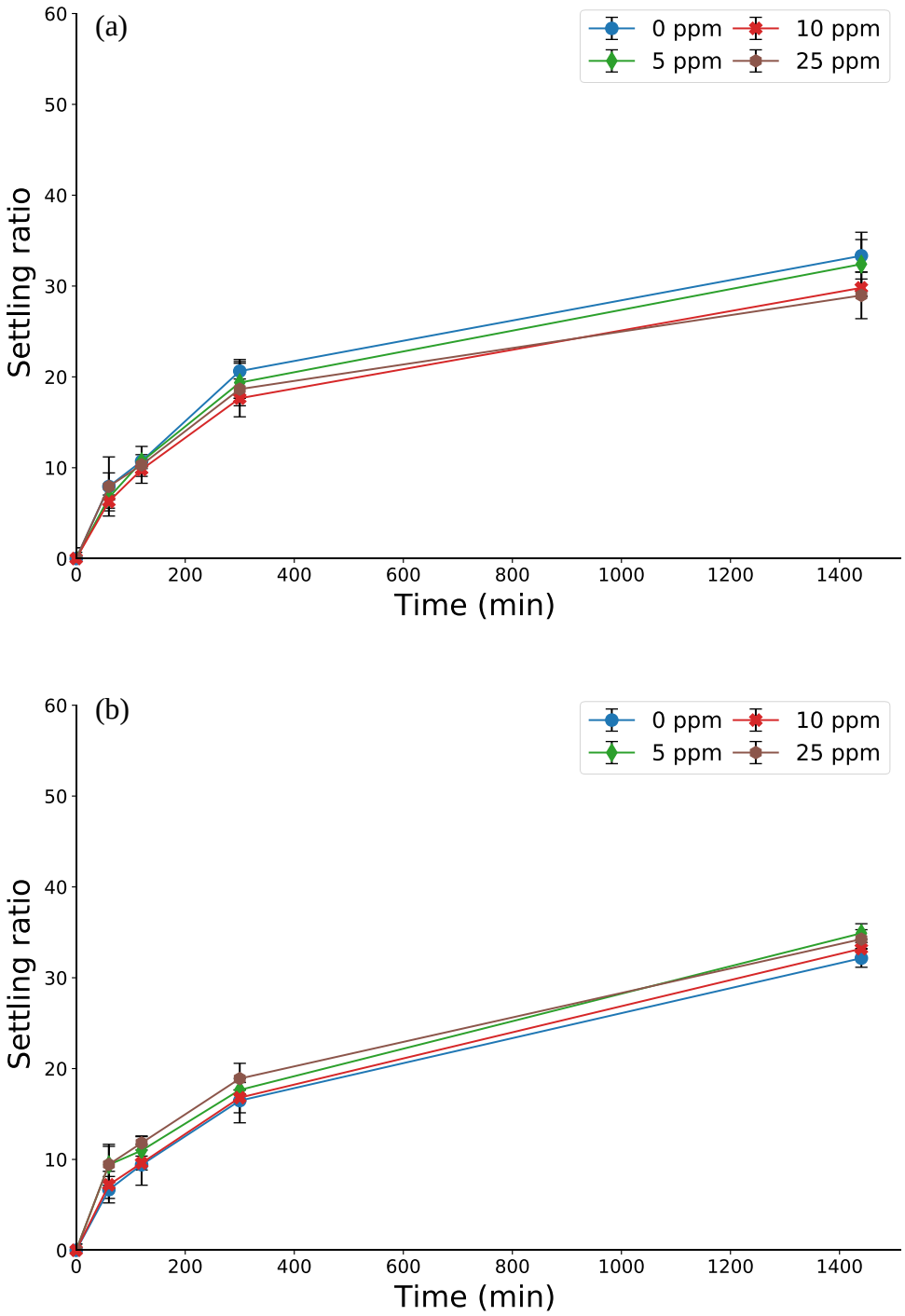

Figure 3-34 Settling ratio of (a) $CaCl_2$, and (b) H_2SO_4 neutralized Fe-oxide dominated bauxite residue after adding 0, 5, 10, 25 ppm (mg SDS/ kg bauxite residue) SDS dissolved in 0.1 M NaCl

4. CONCLUSIONS

A bauxite residue storage pond over 50 years at an undisclosed non-operational alumina plant was investigated for its properties (pH, EC, water content, and mineral compositions), alkalinity neutralization, and settling improvement after neutralization.

The bauxite residues were characterized by high-water content (> 100%), high pH (> 10) and high salinity (> 2 mS/cm). The lower pH of disposal lake water and surface bauxite residue compared with typically Bayer liquor (pH ~ 12) could be explained by carbonation from atmospheric carbon dioxide to form carbonate and bicarbonate buffer ions during storage. Titration and lake water analysis results suggested that the carbonate/bicarbonate buffer controlled both the liquid phase of bauxite residues and lake water. Major minerals in bauxite residues were Fe-oxides (hematite, goethite), Al-oxides (boehmite, gibbsite, bayerite, nordstrandite), calcite, and quartz. Two major groups of bauxite residue samples—Fe-oxide and Al-oxide dominated—were identified based on mineralogical compositions.

Decreased pH during storage was believed to induce the formation of uncommon Al-rich crust and upper layer in the disposal pond. Hard surface crust, consisting bayerite, nordstrandite, and calcite, was found in the land area. Their formation could be attributed to two mechanisms: (1) local pH reduction driven by calcite formation; (2) preferred crystallization induced by high sodium concentration under evaporation conditions. Unusual Al-oxide dominated bauxite residue in the top section of the disposal lake contained bayerite, nordstrandite, gibbsite, hematite, and goethite. The

enrichment of aluminum hydroxides might have resulted from the lower pH of lake water, which promoted the formation of aluminum hydroxide minerals. Precipitation of aluminum hydroxide minerals reduced the aluminate concentration locally, further promoted the diffusion of the aluminate ions in the pore water underneath residues to the water-bauxite residues interface.

Various alkalinity neutralized treatments, including $CaCl_2$, $FeCl_3$, H_2SO_4 and NaH_2PO_4, for bauxite residue were examined. All treatments could successfully decrease the pH to 8 or lower. Loosely distributed particles on the glass slides and smaller particles under optical microscope were observed and indicated the breakdown of macro-aggregate after neutralization treatments. The XRD, FTIR and particle size analysis showed no significant difference in mineral compositions before and after all alkalinity neutralization treatments. Although reducing pH (H_2SO_4), adding polyvalent cations ($CaCl_2$, $FeCl_3$), using phosphate (NaH_2PO_4) as cementing material were hypothetically capable of accelerating the flocculation and aggregation, none of these treatments improved the settling of the residue when compared to 0.1 M NaCl control.

Surfactant SDS could enhance the settling performance of untreated bauxite residue. After alkalinity neutralizing, surfactant SDS lost the ability to accelerate the settling, which could be attributed to the precipitation of the surfactant by the calcium ions or the higher adsorption at neutral pH. Although the smaller particles mentioned above might reduce the efficiency of SDS, the complete lack of settling improvement suggested that the surface alternation by the reduced pH.

The poor ability of cationic PAM to improve settling was due to the strong affinity of cationic PAM on negative charge particle surface. Neutral and anionic PAM could promote the flocculation and settling of bauxite residue both before and after alkalinity neutralization. Significant settling improvement on $CaCl_2$, $FeCl_3$, H_2SO_4 neutralized Fe-oxide dominated bauxite residue by neutral and anionic PAM were observed. Poor performance on NaH_2PO_4 treated Fe-oxide dominated bauxite residue could be explained by the change of surface properties from phosphate ions. After adding PAM, large flocs formed in the tubes resulting in the low settling ratio for $CaCl_2$, $FeCl_3$ and H_2SO_4 neutralized bauxite residue. Although some treatments showed promising enhancement in terms of settling ratio in the initial stage, the final consolidation volumes of bauxite residue after adding PAM increased. Expected synergistic effect of cation (Ca^{2+}, Fe^{3+}) and PAM on settling was not observed, and pH might be the dominant factor affecting settling from two-way ANOVA analysis.

The results suggest that both alkalinity neutralization and calcite formation could reduce the pH of the residue. Reducing the pH of the residue alone would not improve its settling. Among the surfactant and polymers tested, anionic and nonionic polyacrylamide could enhance the settling of residue by forming larger flocs more quickly. Forming stable large flocs also promoted the formation of large pores, which hindered the consolidation of the particles to smaller volumes.

REFERENCES

1. Klauber, C.; Grafe, M.; Power, G., Bauxite residue issues: II. options for residue utilization. *Hydrometallurgy* **2011,** *108* (1-2), 11-32.

2. Evans, K., The History, Challenges, and New Developments in the Management and Use of Bauxite Residue. *J. Sust. Metall.* **2016,** *2* (4), 316-331.

3. Gräfe, M.; Power, G.; Klauber, C., Bauxite residue issues: III. Alkalinity and associated chemistry. *Hydrometallurgy* **2011,** *108* (1-2), 60-79.

4. Gomes, H. I.; Mares, W. M.; Rogerson, M.; Stewart, D. I.; Burke, I. T., Alkaline residues and the environment: a review of impacts, management practices and opportunities. *Journal of Cleaner Production* **2016,** *112*, 3571-3582.

5. Ruyters, S.; Mertens, J.; Vassilieva, E.; Dehandschutter, B.; Poffijn, A.; Smolders, E., The Red Mud Accident in Ajka (Hungary): Plant Toxicity and Trace Metal Bioavailability in Red Mud Contaminated Soil. *Environmental Science & Technology* **2011,** *45* (4), 1616-1622.

6. Mayes, W. M.; Burke, I.; Gomes, H.; Anton, Á.; Molnár, M.; Feigl, V.; Ujaczki, É., Advances in understanding environmental risks of red mud after the Ajka spill, Hungary. *J. Sust. Metall.* **2016,** *2* (4), 332-343.

7. Verma, A. S.; Suri, N. M.; Kant, S., Applications of bauxite residue: A mini-review. *Waste Manage. Res.* **2017,** *35* (10), 999-1012.

8. Kong, X.; Tian, T.; Xue, S.; Hartley, W.; Huang, L.; Wu, C.; Li, C., Development of alkaline electrochemical characteristics demonstrates soil formation in bauxite residue undergoing natural rehabilitation. *Land Degradation & Development* **2018,** *29* (1), 58-67.

9. Alam, S.; Das, B. K.; Das, S. K., Dispersion and Sedimentation Characteristics of Red Mud. *J. Hazard. Toxic Radioact. Waste* **2018,** *22* (4), 10.

10. Jones, B. E. H.; Haynes, R. J., Bauxite Processing Residue: A Critical Review of Its Formation, Properties, Storage, and Revegetation. *Critical Reviews in Environmental Science and Technology* **2011,** *41* (3), 271-315.

11. Hanahan, C.; McConchie, D.; Pohl, J.; Creelman, R.; Clark, M.; Stocksiek, C., Chemistry of seawater neutralization of bauxite refinery residues (red mud). *Environmental Engineering Science* **2004,** *21* (2), 125-138.

12. Khaitan, S.; Dzombak, D. A.; Lowry, G. V., Chemistry of the Acid Neutralization Capacity of Bauxite Residue. *Environmental Engineering Science* **2009,** *26* (5), 873-881.

13. Courtney, R. G.; Timpson, J. P., Reclamation of fine fraction bauxite processing residue (red mud) amended with coarse fraction residue and gypsum. *Water Air and Soil Pollution* **2005,** *164* (1-4), 91-102.

14. Khaitan, S.; Dzombak, D. A.; Lowry, G. V., Mechanisms of Neutralization of Bauxite Residue by Carbon Dioxide. *J. Environ. Eng.-ASCE* **2009,** *135* (6), 433-438.

15. Wang, C.; Harbottle, D.; Liu, Q. X.; Xu, Z. H., Current state of fine mineral tailings treatment: A critical review on theory and practice. *Miner. Eng.* **2014,** *58*, 113-131.

16. Power, G.; Gräfe, M.; Klauber, C., Bauxite residue issues: I. Current management, disposal and storage practices. *Hydrometallurgy* **2011,** *108* (1-2), 33-45.

17. Liu, Y. J.; Naidu, R.; Ming, H., Surface electrochemical properties of red mud (bauxite residue): Zeta potential and surface charge density. *Journal of Colloid and Interface Science* **2013,** *394*, 451-457.

18. Doroszkowski, A., 6 - The physical chemistry of dispersion. In *Paint and Surface Coatings (Second Edition)*, Lambourne, R.; Strivens, T. A., Eds. Woodhead Publishing: 1999; pp 198-242.

19. Kirwan, L. J.; Hartshorn, A.; McMonagle, J. B.; Fleming, L.; Funnell, D., Chemistry of bauxite residue neutralisation and aspects to implementation. *International Journal of Mineral Processing* **2013,** *119*, 40-50.

20. Palmer, S. J.; Frost, R. L., Characterisation of bauxite and seawater neutralised bauxite residue using XRD and vibrational spectroscopic techniques. *Journal of Materials Science* **2009,** *44* (1), 55-63.

21. Kong, X.; Li, M.; Xue, S.; Hartley, W.; Chen, C.; Wu, C.; Li, X.; Li, Y., Acid transformation of bauxite residue: Conversion of its alkaline characteristics. *J Hazard Mater* **2017,** *324* (Pt B), 382-390.

22. Gangadhara Reddy, N.; Hanumantha Rao, B., Characterization of Settled Particles of the Red Mud Waste Exposed to Different Aqueous Environmental Conditions. *Indian Geotechnical Journal* **2018,** *48* (3), 405-419.

23. Wei, H.; Gao, B. Q.; Ren, J.; Li, A. M.; Yang, H., Coagulation/flocculation in dewatering of sludge: A review. *Water Research* **2018,** *143*, 608-631.

24. Teh, C. Y.; Budiman, P. M.; Shak, K. P. Y.; Wu, T. Y., Recent Advancement of Coagulation-Flocculation and Its Application in Wastewater Treatment. *Industrial & Engineering Chemistry Research* **2016,** *55* (16), 4363-4389.

25. El Samrani, A. G.; Lartiges, B. S.; Montarges-Pelletier, E.; Kazpard, V.; Barres, O.; Ghanbaja, J., Clarification of municipal sewage with ferric chloride: the nature of coagulant species. *Water Research* **2004,** *38* (3), 756-768.

26. Elzinga, E. J.; Sparks, D. L., Phosphate adsorption onto hematite: an in situ ATR-FTIR investigation of the effects of pH and loading level on the mode of phosphate surface complexation. *J Colloid Interface Sci* **2007,** *308* (1), 53-70.

27. Castaldi, P.; Silvetti, M.; Garau, G.; Deiana, S., Influence of the pH on the accumulation of phosphate by red mud (a bauxite ore processing waste). *Journal of Hazardous Materials* **2010,** *182* (1-3), 266-272.

28. Gimsing, A. L.; Borggaard, O. K., Phosphate and glyphosate adsorption by hematite and ferrihydrite and comparison with other variable-charge minerals. *Clays and Clay Minerals* **2007,** *55* (1), 108-114.

29. Lapointe, M.; Barbeau, B., Understanding the roles and characterizing the intrinsic properties of synthetic vs. natural polymers to improve clarification through interparticle Bridging: A review. *Separation and Purification Technology* **2020,** *231*, 25.

30. Patra, A. S.; Makhija, D.; Mukherjee, A. K.; Tiwari, R.; Sahoo, C. R.; Mohanty, B. D., Improved dewatering of iron ore fines by the use of surfactants. *Powder Technology* **2016,** *287*, 43-50.

31. Clifton, M.; Nguyen, T.; Frost, R., Effect of ionic surfactants on bauxite residues suspensions viscosity. *J Colloid Interface Sci* **2007,** *307* (2), 572-7.

32. Bai, B.; Hankins, N. P.; Hey, M. J.; Kingman, S. W., In Situ Mechanistic Study of SDS Adsorption on Hematite for Optimized Froth Flotation. *Industrial & Engineering Chemistry Research* **2004,** *43* (17), 5326-5338.

33. Shukla, S.; S., N., A Review ON K-means DATA Clustering APPROACH. *International Journal of Information & Computation Technology* **2014,** *4* (17), 1847-1860.

34. Arthur, D.; Vassilvitskii, S.; Siam/Acm, k-means plus plus : The Advantages of Careful Seeding. *Proceedings of the Eighteenth Annual Acm-Siam Symposium on Discrete Algorithms* **2007**, 1027-1035.

35. Yuan, C.; Yang, H., Research on K-value selection method of K-means clustering algorithm. *J—Multidisciplinary Scientific Journal* **2019,** *2* (2), 226-235.

36. Luo, M.; Qi, X.; Zhang, Y.; Ren, Y.; Tong, J.; Chen, Z.; Hou, Y.; Yeerkebai, N.; Wang, H.; Feng, S.; Li, F., Study on dealkalization and settling performance of red mud. *Environ Sci Pollut Res Int* **2017,** *24* (2), 1794-1802.

37. Assaad, H. I.; Hou, Y. Q.; Zhou, L.; Carroll, R. J.; Wu, G. Y., Rapid publication-ready MS-Word tables for two-way ANOVA. *Springerplus* **2015,** *4*.

38. Liu, Y.; Lin, C. X.; Wu, Y. G., Characterization of red mud derived from a combined Bayer Process and bauxite calcination method. *Journal of Hazardous Materials* **2007,** *146* (1-2), 255-261.

39. Khaitan, S.; Dzombak, D. A.; Swallow, P.; Schmidt, K.; Fu, J.; Lowry, G. V., Field Evaluation of Bauxite Residue Neutralization by Carbon Dioxide, Vegetation, and Organic Amendments. *J. Environ. Eng.-ASCE* **2010,** *136* (10), 1045-1053.

40. Kong, X.; Guo, Y.; Xue, S.; Hartley, W.; Wu, C.; Ye, Y.; Cheng, Q., Natural evolution of alkaline characteristics in bauxite residue. *Journal of Cleaner Production* **2017,** *143*, 224-230.

41. Kiss, A. B.; Keresztury, G.; Farkas, L., RAMAN AND IR-SPECTRA AND STRUCTURE OF BOEHMITE (GAMMA-ALOOH) - EVIDENCE FOR THE RECENTLY DISCARDED D-2H(17) SPACE GROUP. *Spectrochimica Acta Part a-Molecular and Biomolecular Spectroscopy* **1980,** *36* (7), 653-658.

42. Borra, C. R.; Pontikes, Y.; Binnemans, K.; Van Gerven, T., Leaching of rare earths from bauxite residue (red mud). *Miner. Eng.* **2015,** *76*, 20-27.

43. Comer, J. B., <Genesis of Jamaican Bauxit.pdf>. *Economic Geology* **1974,** *69*, 1251-1264.

44. Chvedov, D.; Ostap, S.; Le, T., Surface properties of red mud particles from potentiometric titration. *Colloids and Surfaces A: Physicochemical and Engineering Aspects* **2001,** *182* (1-3), 131-141.

45. Santini, T.; Fey, M.; Gilkes, R., Experimental Simulation of Long Term Weathering in Alkaline Bauxite Residue Tailings. *Metals* **2015,** *5* (3), 1241-1261.

46. Rodgers, K. A.; Gregory, M. R.; Barton, R., Bayerite, Nordstrandite, Gibbsite, Brucite, and Pseudoboehmite in Discharged Caustic Waste from Campbell Island, Southwest Pacific. *Clays and Clay Minerals* **1991,** *39* (1), 103-107.

47. Schoen, R.; Roberson, C. E., Structures of aluminum hydroxide and geochemical implications. *American Mineralogist* **1970,** *55* (1-2), 43-77.

48. Shayanfar, S.; Aghazadeh, V.; Beyragh, A. S., Thermodynamic Modeling and Experimental Studies of Bayerite Precipitation from Aluminate Solution: Temperature and pH Effect. *Iranian Journal of Chemistry & Chemical Engineering-International English Edition* **2019,** *38* (2), 229-238.

49. Gong, X. Y.; Nie, Z. M.; Qian, M. X.; Liu, J.; Pederson, L. A.; Hobbs, D. T.; McDuffie, N. G., Gibbsite to boehmite transformation in strongly caustic and nitrate environments. *Industrial & Engineering Chemistry Research* **2003,** *42* (10), 2163-2170.

50. Kovács-Pálffy, P.; Velledits, F.; Kónya, P.; Földvári, M.; Sólymos, K. G., Nordstrandite, a new occurrence from Hungary. *Acta Mineralogica-Petrographica* **2008,** *48*, 43-48.

51. Barnhisel, R.; Rich, C., Gibbsite, bayerite, and nordstrandite formation as affected by anions, pH, and mineral surfaces. *Soil Sci. Soc. Am. J.* **1965,** *29* (5), 531-534.

52. Dani, N., Nordstrandite in Bauxite Derived from Phonolite, Lages, Santa Catarina, Brazil. *Clays and Clay Minerals* **2001,** *49* (3), 216-226.

53. Page, J. S.; Reynolds, J. G.; Ely, T. M.; Cooke, G. A., Development of a carbonate crust on alkaline nuclear waste sludge at the Hanford site. *Journal of Hazardous Materials* **2018,** *342*, 375-382.

54. Colleen, H.; David, M.; John, P.; Robert, C.; Malcolm, C.; Curt, S., Chemistry of Seawater Neutralization of Bauxite Refinery Residues (Red Mud). *Environmental Engineering Science* **2004,** *21* (2), 125-138.

55. Menzies, N. W.; Fulton, I. M.; Morrell, W. J., Seawater neutralization of alkaline bauxite residue and implications for revegetation. *J. Environ. Qual.* **2004,** *33* (5), 1877-1884.

56. Zhu, F.; Huang, N.; Xue, S.; Hartley, W.; Li, Y.; Zou, Q., Effects of binding materials on microaggregate size distribution in bauxite residues. *Environ. Sci. Pollut. Res.* **2016,** *23* (23), 23867-23875.

57. McGuire, M. J.; Addai-Mensah, J.; Bremmell, K. E., The effect of polymer structure type, pH and shear on the interfacial chemistry, rheology and dewaterability of model iron oxide dispersions. *Colloids and Surfaces A: Physicochemical and Engineering Aspects* **2006,** *275* (1-3), 153-160.

58. Motin, M. A.; Mia, M. A. H.; Islam, A., Thermodynamic properties of Sodium Dodecyl Sulfate aqueous solutions with Methanol, Ethanol, n-Propanol and iso-Propanol at different temperatures. *Journal of Saudi Chemical Society* **2015,** *19* (2), 172-180.

59. Rahman, A.; Brown, C. W., EFFECT OF PH ON THE CRITICAL MICELLE CONCENTRATION OF SODIUM DODECYL-SULFATE. *Journal of Applied Polymer Science* **1983,** *28* (4), 1331-1334.

60. Baviere, M.; Bazin, B.; Aude, R., CALCIUM EFFECT ON THE SOLUBILITY OF SODIUM DODECYL-SULFATE IN SODIUM-CHLORIDE SOLUTIONS. *Journal of Colloid and Interface Science* **1983,** *92* (2), 580-583.